Estimation of Cross Sectional Distortion in Bending of Rectangular Steel Tubes

HÄMEEN AMMATTIKORKEAKOULU
HÄME UNIVERSITY OF APPLIED SCIENCES

Bachelor's thesis

Mechanical Engineering and Production Technology
(HAMK)

Riihimäki, Spring 2019

Amirali Moradi Chargari

HÄMEEN AMMATTIKORKEAKOULU
HÄME UNIVERSITY OF APPLIED SCIENCES

Mechanical Engineering and Production Technology
Riihimäki

Author Amirali Moradi Chargari **Year** 2019

Subject Estimation of cross sectional distortion in bending of rectangular steel tubes

Supervisor Esa Murtola

ABSTRACT

The current study was commissioned by steel manufacturing company SSAB. Tubes with a rectangular section have the advantages of light weight, high strength, save of material and ease of installation, and they are the key components in frame structures, so they have a wide range of applications.

Wherever tubes are used, an accurate bend angle and an uniform cross section are often desired. As a result, a number of bending processes have been developed for various bending purposes. Rotary draw bending and roll bending are among the most common processes in tube bending. Tubes with a rectangular cross section can easily produce cross-sectional distortion in the bending process, which affects the forming accuracy and appearance of the final product. Factors such as material properties, bending technique and set up as well as geometrical parameters can affect the final quality of the tube.

Many scientists have studied the sectional distortion of tubes with a rectangular cross section in the bending process. They have investigated the effect of different parameters through experimental and mathematical models and tried to eliminate or reduce undesired deformation to optimize the bending result.

In this project the effect of steel grade was examined. Moreover a comparison were made between the distortion on cross section using different mandrel in rotary draw bending (RDB) and roll bending process in two bend angle by utilizing optical measuring devices. Finally finite element analysis was implemented to estimate the distortion and to be compared to the experimental results.

Keywords Bending, finite element, optical measurement, rectangular steel tube

Pages 42 pages

CONTENTS

1 INTRODUCTION

Thin-walled tubes (TWT) have the advantages of being lightweight and having a high bending rigidity, which make them suitable both for general structures with curved parts and for specific applications such as automotive or aerospace components. Their application ranges from simple household items to sophisticated aerospace parts (Figure 1). Wherever tubes are used, accurate bend angle and uniform cross section are often desired. As a result, number of bending processes have been developed for various bending purposes. Rotary draw bending and roll bending are among the most common processes in tube bending. Factors such as tube material characteristic and bending techniques and set up has an effect in final quality of the tube.

Many studies have investigated the effect of different parameters on bending quality and how to minimize bending defects such as wrinkling and cross sectional distortions. (Corona 2004), (Paulsen & Welo, 2001), (Utsumi & Sakaki, 2002), (Liu, 2007), (Hongliang, 2016), (Peng, 2012). Their Studies utilized various methods to analyse the behaviour of the material and the bending process. Finite element analysis (FEA) besides experimental observations has played an important role to predict and improve the bending techniques. Optical measurement systems for Inspection and research is replacing the traditional technique because of several crucial advantages such as fast measurement of parts, even with complex shapes, high data density and, above all, independence of results on part's rigidity. ARAMIS and ATOS are two optical measuring system use for geometrical inspection and strain analysis.

This thesis was done to find cross sectional defects in rectangular tubes using rotary draw bending and roll bending techniques. In addition, distortion and strain in bending were estimated using FEA and the results were compared to the experimental values.

Figure 1. Tubes application in various industries (gas and oil, automotive and aerospace)

2 THEORY

2.1 Tube bending process

There are many ways by which a tube can be bent into the required radius. The main techniques by which tube can be bent into the desired shape are rotary draw bending, compression bending, roll bending and stretch bending. The selection of technique depends upon the following factors:
1. The quality of the bend and production rate desired.
2. Tube's diameter, height, wall thickness and minimum bend radius desired. Table 1 compare general criteria in which one you can choose the desired bending method (Kervick, 1966)

Table 1. characteristics of Bending methods

	Radius	Angle	Accuracy	Cost
Draw bending	Small	180	High	Moderate
Roll bending	Big	360	Low	Low

2.1.1 Rotary draw tube bending

Rotary draw tube bending is the most flexible bending method and is used immensely in industry on account of its tooling and low cost. The tooling consists of a bend die, clamp die, pressure die and wiper die. In this bending technique the tube is securely clamped to the bend die by using the clamp die. The bend die rotates and draws the tube along with it. The pressure die prevents the tube from rotating along with the bend die. The pressure die may be stationary or it may move along with tube. The pressure die provides a boost (pushes the material at the extrados of the tube) to reduce the thinning of the tube and can be very helpful when the bending angle is large and the bending radius is small. A mandrel along with wiper die may be used to prevent the wrinkling and collapse of the tube. But the use of mandrel should be avoided if possible since it increases the production cost. Figure 2 shows the tooling of rotary draw bending process. Rotary draw bending provides close control of metal flow necessary for small radius and thin walled tube (the fabricator 2014).

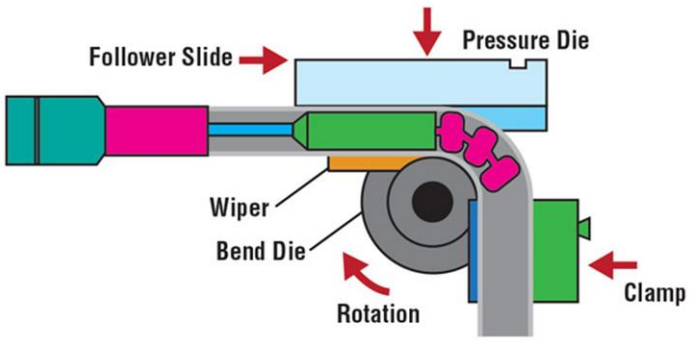

Figure 2. Draw bend machine components (the fabricator 2014).

2.1.2 Roll bending

During the roll bending process the pipe, extrusion, or solid is passed through a series of rollers (typically three) that apply pressure to the pipe gradually changing the bend radius in the pipe (Figure 3). The pyramid style roll benders have one moving roll, usually the top roll. Double pinch type roll benders have two adjustable rolls, usually the bottom rolls, and a fixed top roll. It is suited to producing coils of pipe as well as long gentle bends like those used in truss systems (the fabricator 2014).

Figure 3. Roll bending machine with circular dies attached to the machine to bend circular tubes.

2.2 **Rectangular tube bending terminology**

2.2.1 Dimensions

Height (*h*), width (*b*) and wall thickness (*t*) are the most important dimensions in rectangular tube. Generally b and h are not equal in rectangular tubes otherwise we call it square tube where *b*=*h*. bend angle and radius of the bent are demonstrated in the Figure 4.

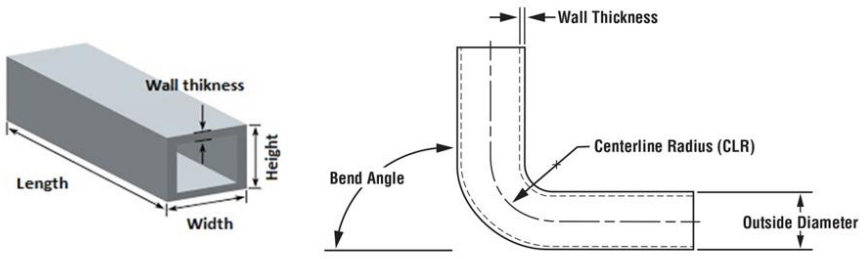

Figure 4. Tube dimensions (the fabricator 2014)

2.2.2 Square versus round corners

Corner radii determine whether a mandrel will fit properly to the inside diameter (ID) of the tube. In some cases, work pieces with rounded corners tend to roll in the direction opposite of the bend radii, causing the material to twist (Figure 5).

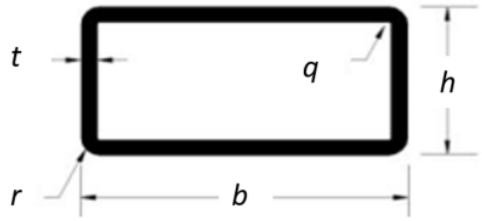

Figure 5. Round corners in a tube

2.3 **Types of distortion in tube bending**

During the bending process, the tube undergoes considerable in-plane distortion. The limitations in the tube bending process are variation in wall thickness, wrinkling, spring back, fracture and distortion of cross-section.

2.3.1 Variation in wall thickness

During the bending process the bending moment induces axial forces in the inner and outer fibres. The inner and outer fibres are subjected to compressive and tensile stresses respectively. This results in thinning of the tube wall at the outer section (extrados) and thickening of the tube wall at the inner section (intrados). The wall thickness variation is shown in Figure 6.

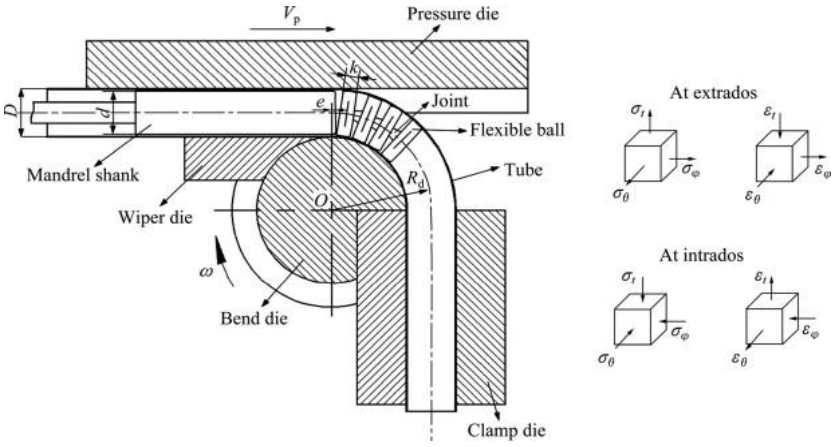

Figure 6. Rotary draw bending process parameters and tube stress-strain states (Yan , Yang , Zhan, et al 2010)

2.3.2 Bursting or fracture

The fibres at the extrados are subjected to tensile stress. When the tensile stress induced in the tube due to the bending moment at the extrados exceeds the ultimate yield strength of the material, the tube fractures at the extrados.

2.3.3 Wrinkling

As a tube is bent, the inner surface of the tube, the intrados is subjected to compressive stress. When the tube is bent into a tight radius, it is subjected to high compressive stress in the intrados which leads to Bifurcation instability or buckling (wrinkling) of the tube (Figure 7). Wrinkles are wavy types of surface distortions. As tubes are used as parts in many applications where tight dimensional tolerances are desired, wrinkles are unacceptable and should be eliminated. Furthermore, wrinkles spoil the aesthetic appearance of the tube.

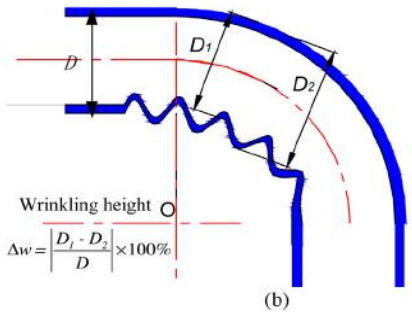

Figure 7. Wrinkling and flattening (Li, Yang, 2014)

2.3.4 Cross section distortion

As described earlier the outer fibres of the tube are subjected to tensile stress whereas inner fibres of the tube are subjected to compressive stress. There is a tendency of fibres at both the ends to move towards the neutral axis. The outer fibre of the tube tends to move towards the neutral plane to reduce the tensile elongation. This results in the cross section of the tube being no longer rectangular, instead being concave in extrados and intrados or oval in circular tubes. The common practice in industry is to provide support to the tube from inside to prevent flattening or distortion of cross section; usually a filler material or mandrel is used for that. Figure 8 shows the cross section distortion of tube.

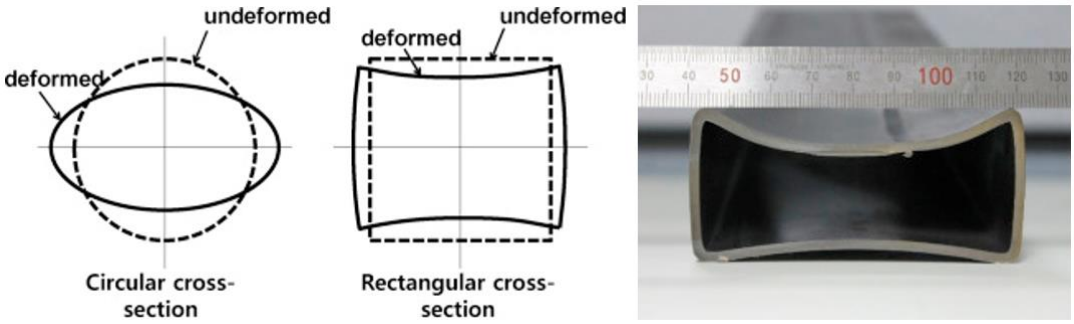

Figure 8. Cross sectional deformations (on the left) and concavity (on the right)

2.3.5 Spring back

After the bending process is complete and the tooling have been withdrawn the bend tube spring backs due to the elastic nature of the tube material. This is called spring back or the elastic recovery of the tube. During the bending process internal stresses are developed in the tube and upon unloading the internal stresses do not vanish. After bending the extrados is subjected to residual tensile stress and the intrados is subjected to residual compressive stress. These residual stresses produce a net internal bending moment which causes spring back. The tube continues to spring back until the internal bending moment drops to zero. The spring back angle depends on the bend angle, tube material, tube size, mandrel, machine and tooling. In actual practice the amount of spring back is calculated and the tube is over bent by that amount. Figure 9 shows the spring back effect after the tooling has been removed.

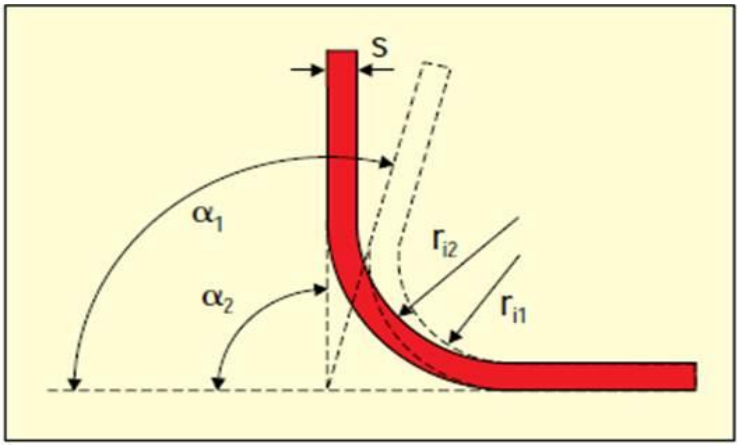

Figure 9. Spring back effect. (α_1 before tool is released and α_2 after tool is released)

2.4 **Mechanics of rectangular tube bending**

2.4.1 Stress-strain curve

The relationship between the stress (σ), force per unit area and strain ,resulting compression/stretching, known as deformation that a particular material displays is known as that particular material's stress–strain curve (Figure 10). It is unique for each material and is found by recording the amount of deformation (strain) (ε) at distinct intervals of tensile or compressive loading (stress). These curves reveal many of the properties of a material (including data to establish the Modulus of Elasticity, E). Stress–strain curves of various materials vary widely, and different tensile tests conducted on the same material yield different results, depending upon the temperature of the specimen and the speed of the loading. It is possible, however, to distinguish some common characteristics among the stress–strain curves of various groups of materials and, on this basis, to divide materials into two broad categories; namely, the ductile materials and the brittle materials.
(https://en.wikipedia.org/wiki/Stress%E2%80%93strain_curve)

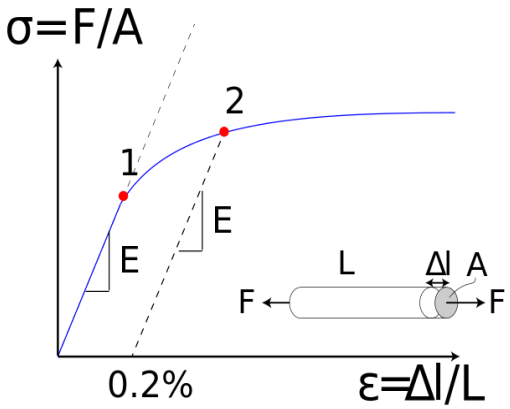

Figure 10. Stress–strain curve showing typical yield behaviour for nonferrous alloys. Stress is shown as a function of strain 1: Elastic (proportionality) limit 2: Offset yield strength (0.2% proof strength).
(https://en.wikipedia.org/wiki/Stress%E2%80%93strain_curve)

2.4.2 Strain rate effect

Two important effects necessary to understand the true stress are the effects of strain rate susceptibility and strain rate hardening upon the true stress. Time is often neglected in the initial stress-strain curve relations, but at higher strain rates, higher stresses will occur. When evaluating steel structures in dynamic cases, which are high speed movements such as fast forming operations or high-speed structural damage such as car accidents

and damage to machinery, it is sometimes worth considering how precision tubes behave. As shown in the Figure 11, It is known that e.g. if, structural steels have strain rate hardening phenomena, which means that the yield strength and flow stress increase as the strain rate increases (SSAB 2016).

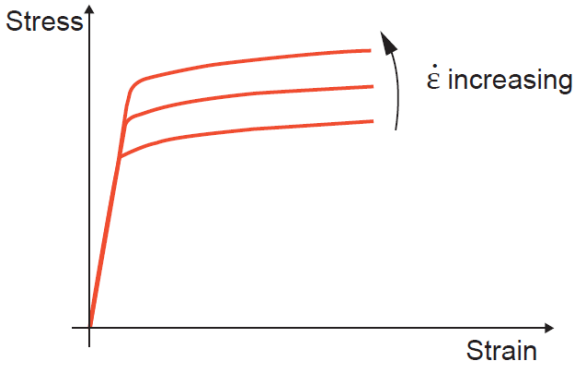

Figure 11. As strain rate increases, yield and ultimate tensile strength increase

2.4.3 Strain hardening

Work hardening, also known as strain hardening, is the strengthening of a metal or polymer by plastic deformation (Figure 12). This strengthening occurs because of dislocation movements and dislocation generation within the crystal structure of the material. Work hardening is a consequence of plastic deformation, a permanent change in shape. This is distinct from elastic deformation, which is reversible. Most materials do not exhibit only one or the other, but rather a combination of the two. (ANSYS tutorial 2018)

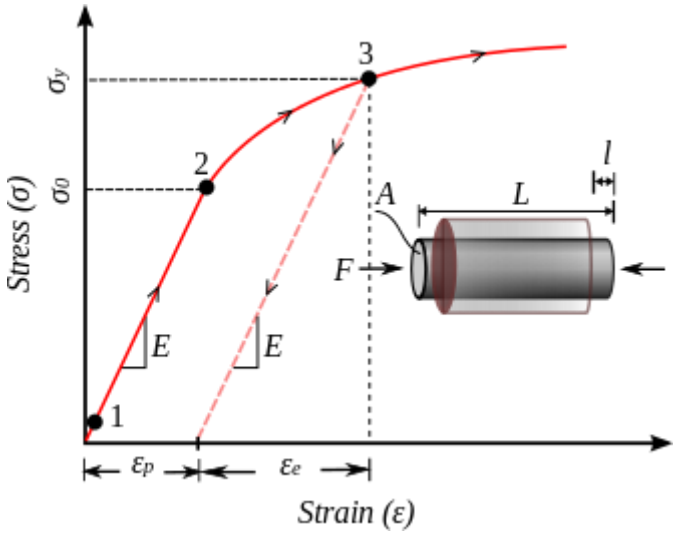

Figure 12. Higher yield strength (3) caused by strain hardening effect

2.4.4 Ductility

The following discussion mostly applies to metals, especially steels, which are well studied. Work hardening occurs most notably for ductile materials such as metals. Ductility is the ability of a material to undergo plastic deformations before fracture (for example, bending a steel rod until it finally breaks). Ductile materials, which includes structural steel and many alloys of other metals, are characterized by their ability to yield at normal temperatures.

Low carbon steel generally exhibits a very linear stress–strain relationship up to a well-defined yield point. The linear portion of the curve is the elastic region and the slope is the modulus of elasticity or Young's Modulus (Young's Modulus is the ratio of the compressive stress to the longitudinal strain). Many ductile materials including some metals, polymers and ceramics exhibit a yield point. Plastic flow initiates at the upper yield point and continues at the lower one. At lower yield point, permanent deformation is heterogeneously distributed along the sample. The deformation band which formed at the upper yield point will propagate along the gauge length at the lower yield point. After the yield point, the curve typically decreases slightly because of dislocations escaping from Cottrell atmospheres. As deformation continues, the stress increases on account of strain hardening until it reaches the ultimate tensile stress.

In tube forming work hardening is rather an undesirable phenomenon hence materials which shows higher ductility and less hardening behaviour consider as an ideal for the process. In the graph below, E235 E220 E190 show a high formability characteristic for bending process (Figure 13). (Podany, Samek, Matousek 2010)

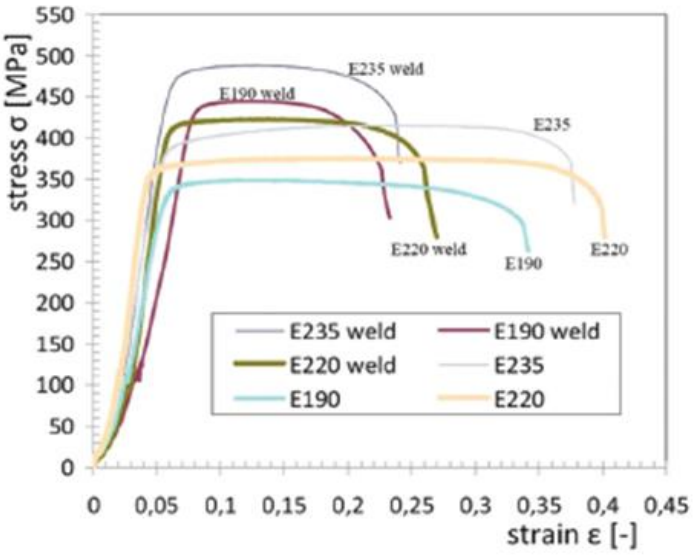

Figure 13. Stress strain curve comparison between different steels (Podany, Samek, Matousek 2010)

2.4.5 Bending stress

A beam deforms and stresses develop inside it when a transverse load is applied on it. In the quasi-static case, the amount of bending deflection and the stresses that develop are assumed not to change over time. In a horizontal beam supported at the ends and loaded downwards in the middle, the material at the top of the beam is compressed while the material at the down side is stretched.

There are two forms of internal stresses caused by lateral loads: Shear stress parallel to the lateral loading plus complementary shear stress on planes perpendicular to the load direction; direct compressive stress in the upper region of the beam, and direct tensile stress in the lower region of the beam. These last two forces form a couple or moment as they are equal in magnitude and opposite in direction. This bending moment resists the sagging deformation characteristic of a beam experiencing bending. The stress distribution in a beam can be predicted quite accurately when some simplifying assumptions are used.

In the Euler–Bernoulli theory of slender beams, a major assumption is that 'plane sections remain plane'. In other words, any deformation due to shear across the section is not accounted for (no shear deformation). Also, this linear distribution is only applicable if the maximum stress is less than the yield stress of the material. The maximum stress experienced in the section (at the furthest points from the neutral axis of the beam) is defined as the flexural strength. Plastic bending begins when an applied moment causes the outside fibres of a cross-section to exceed the material's yield strength. Loaded only by a moment, the peak bending stresses occurs at the outside fibres of a cross-section. The cross-section will not yield linearly through the section. Rather, outside regions will yield first, redistributing stress and delaying failure beyond what would be predicted by elastic analytical methods. The stress distribution from the neutral axis is the same as the shape of the stress-strain curve of the material (Figure 14). After a cross-section reaches a sufficiently high condition of plastic bending, it acts as a Plastic hinge. (https://en.wikipedia.org/wiki/Bending)

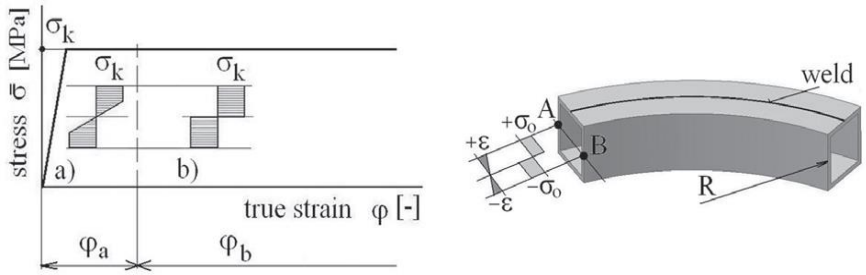

Figure 14. Linear approximation of the flow stress (Podany, Samek, Matousek 2010)

2.4.6 Elasticity

Before proceeding to a discussion on plasticity, it may be useful to review elasticity of metals. In elastic response, if the induced stresses are below the material's yield strength, the material can fully recover its original shape upon unloading. From a standpoint of metals, this behaviour is due to the stretching but not breaking of chemical bonds between atoms. Because elasticity is due to this stretching of atomic bonds, it is fully recoverable. Moreover, these elastic strains tend to be small. (ANSYS tutorial 2018) Elastic behaviour of metals is most commonly described by the stress-strain relationship of Hooke's Law: $\sigma = E\epsilon$

2.4.7 Plasticity

When a ductile material experiences stresses beyond the elastic limit, it will yield, acquiring large permanent deformations (Figure 15).

- Plasticity refers to the material response beyond yield.
- Plastic response is important for metal forming operations.
- Plasticity is also important as an energy-absorbing mechanism for structures in service.
- Materials that fail with little plastic deformation are said to be brittle.
- Ductile response is safer in many respects than is brittle response.

Plastic deformation results from slip between planes of atoms due to shear stresses (deviatoric stresses). This dislocation motion is essentially atoms in the crystal structure rearranging themselves to have new neighbours results in unrecoverable strains or permanent deformation after load is removed. Slipping does not generally result in any volumetric strains (condition of incompressibility), unlike elasticity.

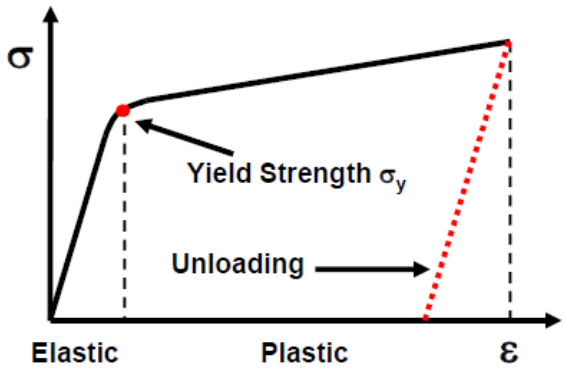

Figure 15. Plastic deformation caused by a load higher than yield strength

2.4.8 Rate-independent plasticity

If the material response is not dependent on the rate of loading or deformation, the material is said to be rate-independent. Most metals

exhibit rate-independent behaviour at low temperatures (< 1/4 or 1/3 melting temperature) and low strain rates.

2.4.9 Yield criterion

The yield criteria is used to relate multiaxial stress state with the uniaxial case. Tensile testing on specimens provide uniaxial data, which can easily be plotted on one-dimensional stress-strain curves, such as those presented earlier in this section. The actual structure usually exhibits multiaxial stress state. The yield criterion provides a scalar invariant measure of the stress state of the material which can be compared with the uniaxial case. In general, a stress state can be separated into two components (Figure 16).

– Hydrostatic stress - generates volume change.
– Deviatoric stress - generates angular distortion.

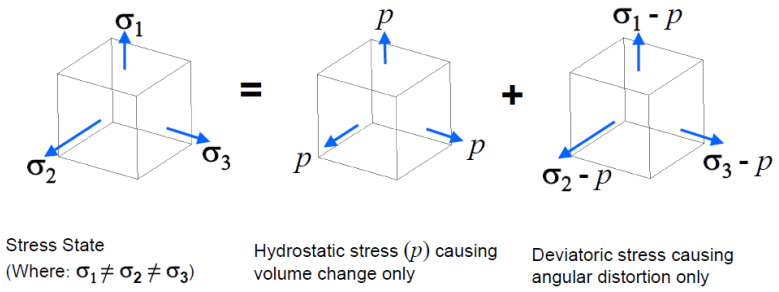

Figure 16. Stress states, Hydrostatic stress and Hydrostatic stress
Ansys tutorial retrieved from:
(http://inside.mines.edu/~apetrell/ENME442/Labs/1301_ENME442_lab7.pdf)

The von Mises yield criterion predicts that yielding will occur whenever the distortion energy in a unit volume equals the distortion energy in the same volume when uniaxial stressed to the yield strength. From this theory, a scalar invariant (von Mises equivalent stress) is derived as:

$$\sigma_e = \sqrt{\frac{1}{2}[(\sigma_1 - \sigma_2)^2 + (\sigma_2 - \sigma_3)^2 + (\sigma_3 - \sigma_1)^2]}$$

2.4.10 Hardening rules

The hardening rule describes how the yield surface changes (size, centre, and shape) as the result of plastic deformation. The hardening rule determines when the material will yield again if the loading is continued or reversed.

This is in contrast to elastic-perfectly-plastic materials which exhibit no hardening -- i.e., the yield surface remains fixed.

As shown in Figure 17 there are two basic hardening rules to prescribe the modification of the yield surface:
Kinematic hardening
• The yield surface remains constant in size and translates in the direction of yielding.
Isotropic hardening.
• The yield surface expands uniformly in all directions with plastic flow.

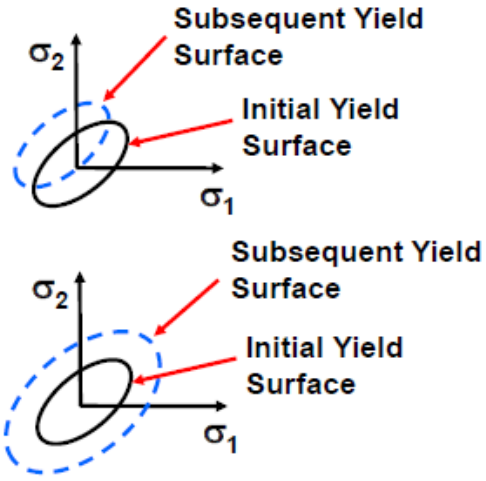

Figure 17. Kinematic hardening (top) and isotropic hardening (down) (http://inside.mines.edu/~apetrell/ENME442/Labs/1301_ENME442_lab7.pdf)

Subsequent yield in compression is decreased by the amount that the yield stress in tension increased, so that a 2σy difference between the yields is always maintained. (This is known as the Bauschinger effect.)
An initially isotropic material is no longer isotropic after it yields and experiences kinematic hardening (Figure 18).

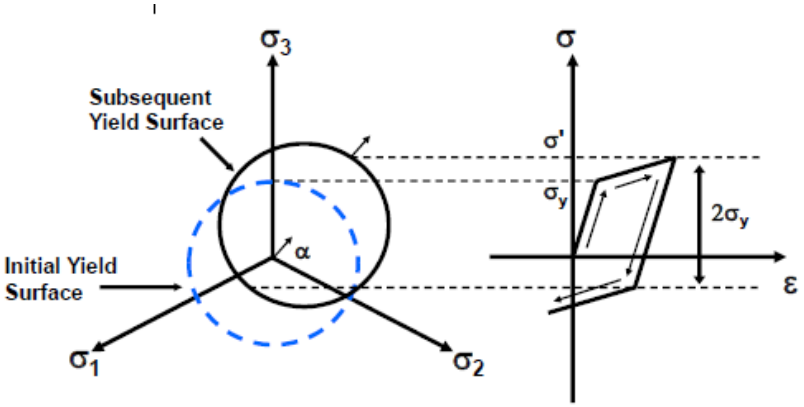

Figure 18. The stress-strain behaviour for linear kinematic hardening (http://inside.mines.edu/~apetrell/ENME442/Labs/1301_ENME442_lab7.pdf)

For very large strain simulations, the linear kinematic hardening model can become inappropriate because of the Bauschinger effect. Kinematic hardening is generally used for small strain, cyclic loading applications.
As shown in Figure 19 isotropic hardening states that the yield surface expands uniformly during plastic flow. The term 'isotropic' refers to the uniform dilatation of the yield surface and is different from an 'isotropic' yield criterion (i.e., material orientation).

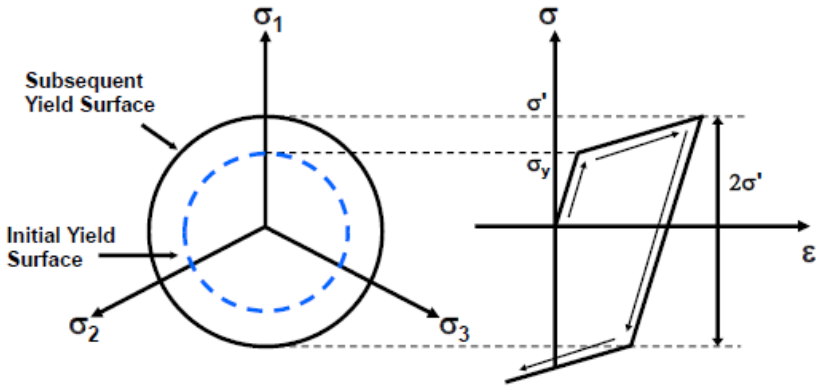

Figure 19. The stress-strain behaviour for isotropic hardening(http://inside.mines.edu/~apetrell/ENME442/Labs/1301_ENME442_lab7.pdf)

Plotting the stress-strain curve enables an understanding of what occurs during a loading and reverse loading cycle: Note that the subsequent yield in compression is equal to the highest stress attained during the tensile phase. Isotropic hardening is often used for large strain or proportional loading simulations. It is usually not applicable for cyclic loading. (ANSYS tutorial 2018 retrieved from: (http://inside.mines.edu/~apetrell/ENME442/Labs/1301_ENME442_lab7.pdf).

2.5 **Finite element method**

2.5.1 Definition

The finite element method (FEM) is a numerical technique for solving problems which are described by partial differential equations or can be formulated as functional minimization. A domain of interest is represented as an assembly of finite elements. Approximating functions in finite elements are determined in terms of nodal values of a physical field which is sought. A continuous physical problem is transformed into a discretized finite element problem with unknown nodal values. For a linear problem a system of linear algebraic equations should be solved. Values inside finite elements can be recovered using nodal values.
Two features of the FEM are worth to be mentioned:

1) Piece-wise approximation of physical fields on finite elements provides good precision even with simple approximating functions (increasing the number of elements we can achieve any precision).
2) Locality of approximation leads to sparse equation systems for a discretized problem. This helps to solve problems with very large number of nodal unknowns.

2.5.2 Process

To summarize in general terms how the finite element method works we here listed the main steps of the finite element solution procedure as follows:
1. Discretize the continuum. The first step is to divide a solution region into finite elements. The finite element mesh is typically generated by a preprocessor program. The description of mesh consists of several arrays main of which are nodal coordinates and element connectivity.
2. Select interpolation functions. Interpolation functions are used to interpolate the field variables over the element. Often, polynomials are selected as interpolation functions. The degree of the polynomial depends on the number of nodes assigned to the element (Nikishkov 2004). Figure 20 shows different element that are used in FEM analysis.

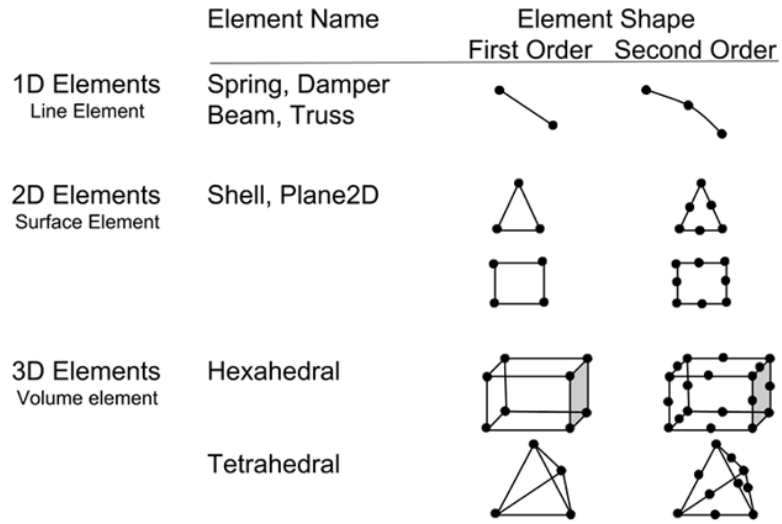

Figure 20. Different 1D, 2D and 3D basic elements Image source: (Holm, 2002)

3. Find the element properties. The matrix equation for the finite element should be established which relates the nodal values of the unknown function to other parameters. For this task different approaches can be used; the most convenient are: the variational approach and the Galerkin method.
4. Assemble the element equations. To find the global equation system for the whole solution region we must assemble all the element equations. In other words we must combine local element equations for all elements used for discretization. Element connectivities are used for the assembly

process. Before solution, boundary conditions (which are not accounted in element equations) should be imposed.
5. Solve the global equation system. The finite element global equation system is typically sparse, symmetric and positive definite. Direct and iterative methods can be used for solution. The nodal values of the sought function are produced as a result of the solution.
6. Compute additional results. In many cases we need to calculate additional parameters. For example, in mechanical problems strains and stresses are of interest in addition to displacements, which are obtained after solution of the global equation system. (Nikishkov 2004)

2.6 **Optical measurement**

The measurement of dimensional and shape precision in industrial practice is about to transform from conventional methods such as a contact method using coordinate measuring machines to noncontact optical measurement systems. Although conventional machines provide one of the most accurate results, they cannot be used in measurement of surfaces with very complex shapes. That is the reason why laser and optical measurement systems, so called 3D scanners, are used more and more often. These scanners digitize the part, and the inspection itself is performed on a virtual model obtained by means of the digitization process. Inspection using these systems offer several crucial advantages such as fast measurement of parts, even with complex shapes, high data density and, above all, independence of results on part's rigidity. Due to the overall description of a measured part, it also allows to perform complex and objective analysis.

Currently, optical 3D scanners are often used as a universal measurement and inspection device. Therefore, the user must be sure that he uses an optical scanner working in a defined range of accuracy. In long-term perspective the only way to meet this requirement is to use comparable criteria and regular inspection of the device (scanner). The manufacturer recommends to perform the acceptance test approximately once a year or more often for specific industries. A more detailed comparison of several scanning systems and assessment of 3D scanner precision was published by Barbero 2011. In order to determine the measurement uncertainty, the team performed measurement of several calibration elements such as sphere, cylinder and gage block. An uncertainty of 25 µm was determined during the Atos system measurement process. Palousek 2015 and His team performing the research found out that while the chalk coating may reach the average thickness up to 44 µm, using titanium-white-based anti-reflection coating reduces the thickness approximately tenfold – down to 5 µm, offering a highly positive effect on the accuracy of digitization process. (Mendricky 2016.)

2.6.1 ATOS COMPACT 5M

The digitizing system ATOS (Advanced Topometric Sensor) digitizes measuring objects fast and easily with a high local measuring point resolution and accuracy. The ATOS system works according to the triangulation principle. The system captures each single 3D measuring point via two different methods in a quasitriangular measurement. During the measurement, the ATOS sensor projects a fringe pattern onto the measuring object which both cameras capture. To digitize a measuring object completely, you need several individual measurements from different directions. Depending on the sensor and the lenses used, a three-dimensional area results at a defined distance in which the system computes 3D points. This area is the measuring volume Table 2 demonstrate the achievable measuring volumes by using different set up. The system transforms the individual measurements into a global coordinate system. To do so, the system uses reference points (circular point markers). You apply the reference points to the measuring object or in the vicinity of the measuring object. If you apply the reference points in the vicinity of the measuring object, you can use e.g. fixtures, rotation Tables or frames.

Table 2. Measuring volumes achievable by ATOS COMPACT 5M (ATOS-Compact manual)

Sensor	Camera position	Name [mm]	Measuring volume (MV) (L x W x H) in mm [mm]	Measuring point distance [mm]	Recommended reference points mm Ø [mm]	Measuring distance [mm]	Camera angle [°]	Focal length camera lenses [mm]	Focal length projector lens [mm]	**Standard calibration objects**, Alternative calibration objects (CP = Panel, CC = Cross)
ATOS COMPACT SCAN 5M Rev. 01	**500**	1200	1200 x 900 x 900	0.481	8	1170	24	8	6	**CP40/MV1000**, CC30/MV1000x1000
		800	800 x 600 x 600	0.325	3	1170	24	12	8	**CP40/MV700**, CC30/MV700
		600	600 x 450 x 450	0.243	3	1170	24	17	12	**CP40/MV560**, CC30/MV500x500
		300	300 x 230 x 230	0.124	1.5	1170	24	35	23	**CP40/MV320**, CC30/MV300
	300	600	600 x 450 x 450	0.250	3	590	25	8	6	**CP40/MV560**, CC30/MV500x500
		300	300 x 230 x 230	0.124	1.5	590	25	17	12	**CP40/MV320**, CC30/MV300
		150	150 x 110 x 110	0.062	0.8	590	25	35	23	**CP40/MV170**
	SO	150	150 x 110 x 110	0.063	0.8	420	23	17	16	**CP40/MV170**
		70	70 x 50 x 50	0.029	0.4	420	23	35	28	**CP40/MV100**
		40	40 x 30 x 20	0.017	0.4	420	23	50	50	**CP40/MV60**

2.6.2 ARAMIS ADJUSTABLE 5

ARAMIS is a non-contact optical 3D deformation measuring system. It analyzes, calculates and documents deformations. The graphical representation of the measuring results provides an optimum understanding of the behavior of the measuring object. ARAMIS recognizes the surface structure of the measuring object in digital camera images and allocates coordinates to the image pixels. The first image in the measuring project represents the undeformed state of the object. After or during the deformation of the measuring object, further images are recorded. Then, ARAMIS compares the digital images and calculates the displacement and deformation of the object characteristics. If the measuring object has only a few object characteristics, like it is the case with homogeneous surfaces, you need to prepare such surfaces by means of suitable methods, for example apply a stochastic color spray pattern.
ARAMIS is particularly suitable for three-dimensional deformation measurements under static and dynamic load in order to analyze deformations and strain of real components. Most of the system functions are controlled by the software. During computation, ARAMIS observes the deformation of the specimen through the images by means of various square or rectangular image details (facets). Figure 21 shows 15 x 15 pixel facets with a 2 pixel overlapping area (ARAMIS adjustable 5 software user manual).

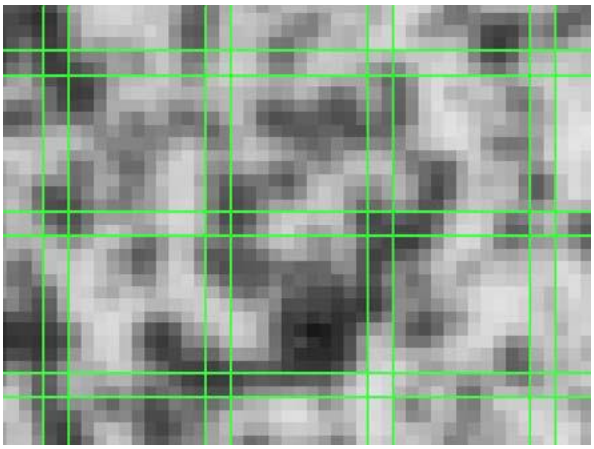

Figure 21. 15x15 facets with 2 pixels overlapping (ARAMIS adjustable 5 software user manual).

The system determines the 2D coordinates of the facets from the corner points of the green facets and the resulting centers. Using photogrammetric methods, the 2D coordinates of a facet, observed from the left camera and the 2D coordinates of the same facet, observed from the right camera, lead to a common 3D coordinate (Figure 22).

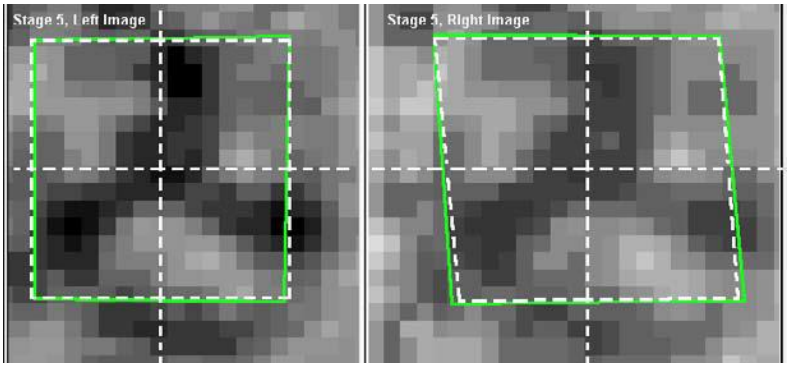

Figure 22. example of facets and image from right and left camera (ARAMIS adjustable 5 software user manual)

Main Hardware and Software Components:

- Sensor with two cameras (only for 3D setup)
- Stand for secure and steady hold of the sensor
- LED specimen lighting (standard for ARAMIS 4M and 5M)
- Laser pointer for optimum sensor adjustment (standard for ARAMIS 4M, 5M and HS systems)
- Sensor controller for power supply of the cameras, control of image recording and inputs for analog signals
- High-performance PC system
- ARAMIS application software and Linux system software

3 SECTIONAL DISTORSION OF TUBES

Many scientists have studied the sectional distortion of tubes with a rectangular cross section in bending process. Corona (Corona 2004) established a theoretical model about section distortion and it is verified by experiment. Paulsen and Welo (2001) studied the impact rule of the cross-sectional shape in bending to the cross-sectional distortion. Utsumi (2002) studied reducing the cross-sectional distortion through using mandrel in rotary draw bending of tubes with rectangular section. Liu (2007) established a three-dimensional finite element analysis model to study the influence of process parameters on the distortion of thin-walled tubes with rectangular cross-section in bending process.

Peng et al. (2012) compared and analyzed sectional distortion of overall bending and bending multi-point bending for the tubes with rectangular section, and have studied the influence of friction coefficient, wall thickness, bend radius to the cross-section distortion while multi-point bending. Hongilang (2016) studied the impact of geometrical parameters on cross section in rotary draw bending of high-strength steel tube with rectangular cross section.

However, the effect of steel grade has not been investigated. Moreover a comparison between distortions on the cross section using a mandrel in rotary draw bending (RDB) has not been studied. Finally utilizing optical measuring devices for inspection has not found in any of the studies. This article studies the cross sectional deformation and analyze strains in hot rolled and cold rolled rectangular steel tubes in RDB with and without mandrel, utilizing optical measuring system. From this point of view, the present work aims to investigate the cross-sectional distortion behaviors of thin-walled rectangular steel alloy tube in rotary-draw bending process by using FEM simulation method combined with theoretical analysis and experimental study.

4 EMPIRICAL PART

4.1 Tubes

Three different rectangular tubes of the same dimension 20x60 mm of the steel manufacturer SSAB was selected, the tubes were varied in thickness and material properties (cold rolled and hot rolled). The tubes have been tested in various bending set up. Table 3 shows the mechanical properties of the tubes where, Re(0.2) = yield stress (MPa), Rm = ultimate tensile strength (MPa) and A% = total elongation at failure.

Table 3. Mechanical properties of the tubes

name	width	height	thickness (mm)	grade	Re(0.2)	Rm	A%	E (GPa)
220C	60	20	2	cold rolled	344	374	44%	210
220C	60	20	1.5	cold rolled	336	378	45%	210
220H	60	20	2	hot rolled	312	359	49%	210

4.2 Bending process

In the bending process, the extruded tube rotates along the grooves of a bend die and clamp die to the desired bending degree and the bending radius, while a sliding pressure die forces the tube to conform to the die radius. The wiper die, the vulnerable part with a very thin feather edge, is often placed behind the bend die to prevent wrinkling of the part. Due to acute contact condition, the edge of the wiper die may be worn heavily.

To avoid abrasion and to extend the life of the wiper die, the rake angle die is set by rotating the die along the bend die cavity away from the line of tangency. The axis force from the boost block can help to minimize the bend tube's wall thickness variance and deformation. Booster force improves the material flow in the forming zone and leads to less thinning of the wall on the outside of the bend and less cross section distortion.

So the process needs precise coordination of various dies and strictly controlling of forming parameters. In addition, a mandrel with flexible cores (Figure 23) is positioned inside the tube to provide rigid support. Three different mandrels were used, two mandrel for tubes with 2 mm thickness and one mandrel for 1.5 mm thickness. The Mandrel's dimensions are shown in Table 4.

Table 4. dimensions of the mandrels

	old 2mm	new 2mm	1.5 mm
width	54	55.5	56.8
thickness	15.1	15.5	16.6

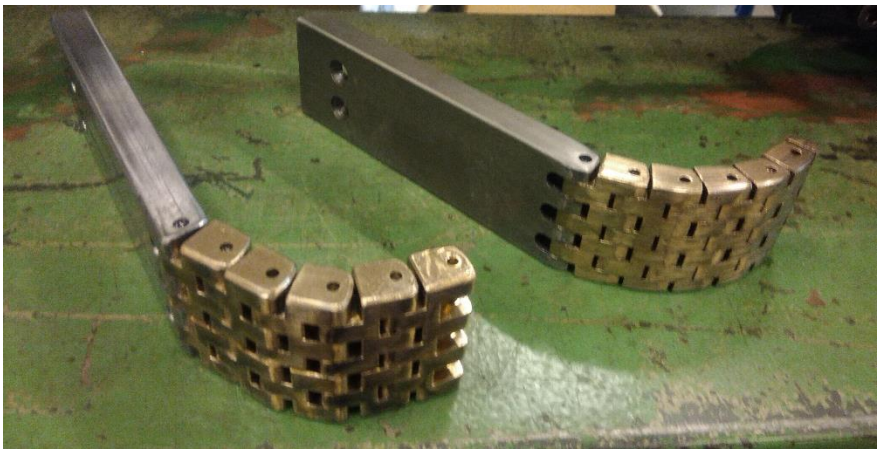

Figure 23. Draw bending mandrels segments made with brass for lower friction and wear out resistance

One test was done without a mandrel and each tubes was bended to two angle (45 and 90 degree) with a bending radius of 50 mm. Besides the draw bending, tubes were bended by rotary draw bending machine into 45 and 90 degree angle by 400 mm bend radius. Five specimen were made for each of the set ups. The clearance between the pressure die and the wiper die with tube was adjusted to zero during all the bending process. The number of samples for each tube is demonstrated in the Table 5 and 6.

Table 5. draw bending samples

		220 (t=2)		220 (t=1.5)
mandrel	bend angle	cold rolled	hot rolled	cold rolled
None	45	1	1	1
	90	1	1	1
Old (t=2 mm)	45	5	5	
	90	5	5	
New (t=2 mm)	45	5	5	
	90	5	5	
New (t=1.5 mm)	45			5
	90			5
	total	22	22	12

Table 6. Roll bends samples

	220 (t=2)		220 (t=1.5)
Bend degree	cold rolled	hot rolled	cold rolled
45	5	5	5
90	5	5	5
total	10	10	10

4.3 **Measurements with ARAMIS**

ARAMIS and analyzing software GOM correlate was used to inspect the deformation and strain on tubes. Aramis is a non-contact optical 3D deformation measuring system. It analyzes, calculates and documents deformations. The graphical representation of the measuring results provides an optimum understanding of the behavior of the measuring object. If the measuring object has only a few object characteristics, like it is the case with homogeneous surfaces (like the surface of our tubes), as it was in our case you need to prepare such surfaces by means of suitable methods, for example apply a stochastic color spray pattern.
The measuring process were as follows:

- choosing the appropriate measuring volume (125x100mm)
- set up lenses (50 mm lens)
- calibration with corresponding panel
- specimen preparation (applying the stochastic pattern)

To achieve a good result all the steps have to be taken precisely and coherently as they are closely related and affect the result. Facet size of 15x15 with 2 pixel overlap is recommended by the manufacturer were chosen and shutter time were set to the 70 ms according to the set up parameters. The maximum frame rate of our Aramis system was 15 image per second. One of the limitation of measuring was the geometry of the bend machines which were blocking the view of the sensor during the bending after few unsuccessful attempt to capture the tube during bending we decided to capture the surface before and after bend. for draw bending we captured the surface before and after bending, and for roll bending we captured five times during the bending so each time tube was bended to certain angle and displaced from the machine to take the picture until it reaches the final angle for the last picture.

4.4 **Scanning with ATOS**

The digitizing system ATOS (Advanced Topometric Sensor) and corresponded Inspection software provided by the manufacturer were utilized for recording of the data and inspection of the deformation. Atos digitizes measuring objects fast and easily with a high local measuring point resolution and accuracy and then polygonise the point cloud into mesh surface, GOM offers a software which can be used for variety of inspection and actual and nominal data comparison. The acceptance test is performed to verify measurement accuracy of optical systems. Based on characteristic parameters, it verifies whether the measurement system meets the quality limit parameters or not. The measured deviations must not exceed the limit values given by the manufacturer, which are specific for various scanner types, measuring volumes and parameters. The ATOS device test is governed by manufacturer's (GOM) specifications and is in accordance with the VDI/VDE 2634 – part 3 [VDI/VDE 2634 2008] standard, related to optical 3D systems.

According to the tube dimensions, the correct measuring volume was selected and the lenses with focal length of 150 mm were chosen. Sensor Calibration was done according to the manufacturer's instructions and the warm-up time was maintained beforehand. After calibration A deviation of 0.03 pixel was reported which is equal to 0.003 mm and it is considered acceptable for scanning. Before scanning the reference points were attached and anti-reflect spray was applied to the surface (Figure 24).

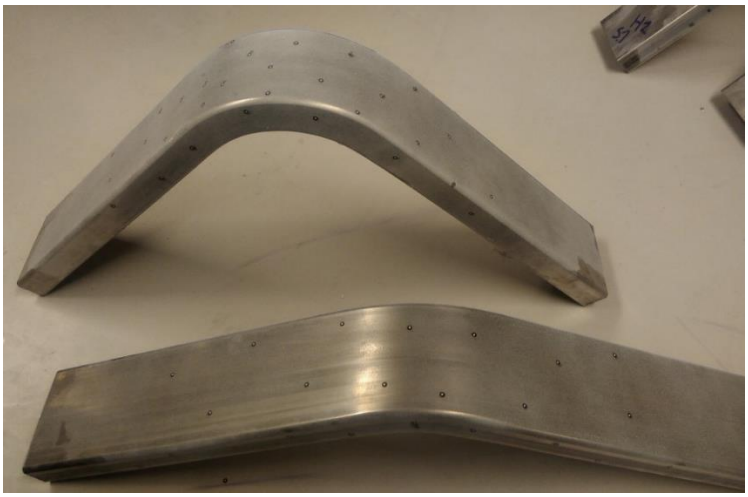

Figure 24. Tubes covered with titanium oxide and attached reference points

4.5 **Inspection**

GOM correlate was used for both ARAMIS and ATOS scans to measure deformation and strain. For ATOS a mesh was created and alignment was done for all the tubes in the same way, sections created and the deformation was measured along the bend from 0 to the final bend angle (45 and 90). Concavity measured from the line that pass through the edges of the tube to the middle (x) as illustrated in Figure25.

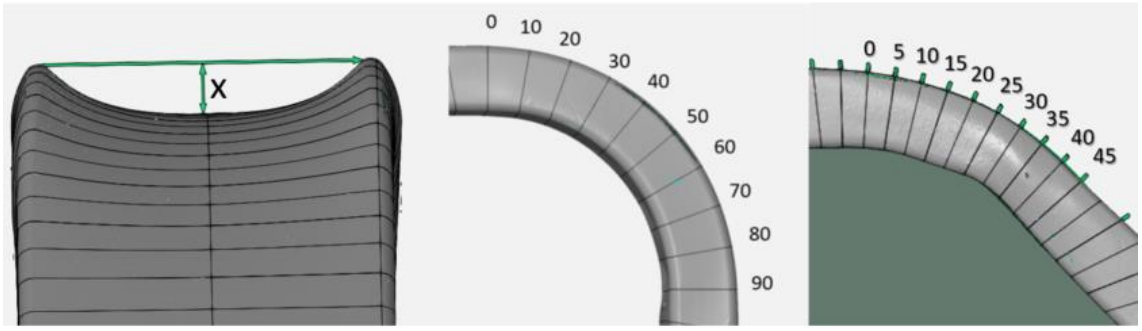

Figure 25. Concavity and bend angle measuring points

Moreover the deformation along the highest value in the line perpendicular to the band direction was measured (transverse) Concavity was measured in transverse direction (edge to edge) every 5mm from the bend point where the maximum concavity was observed (Figure 26).

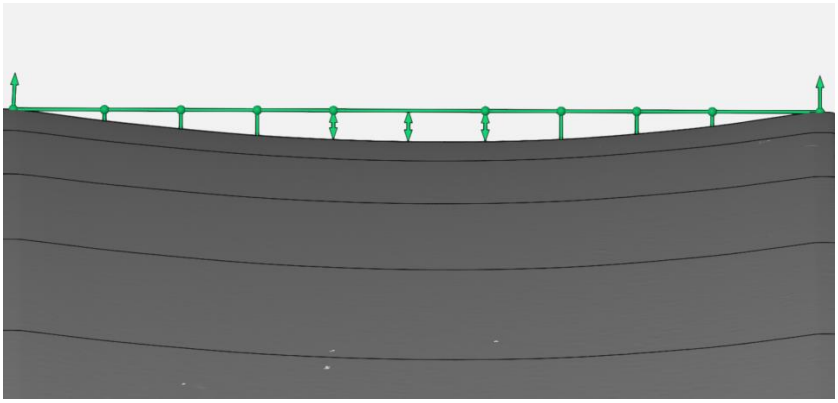

Figure 26. Measuring concavity distortion along the transverse direction

For the results derived from ARAMIS, facet points (surface component) were created (Figure 27) and after that tubes were aligned with the same way. Vons Misses stress was measured on the whole surface in a longitudinal line along the bend direction and in a transverse line perpendicular to the bend direction.

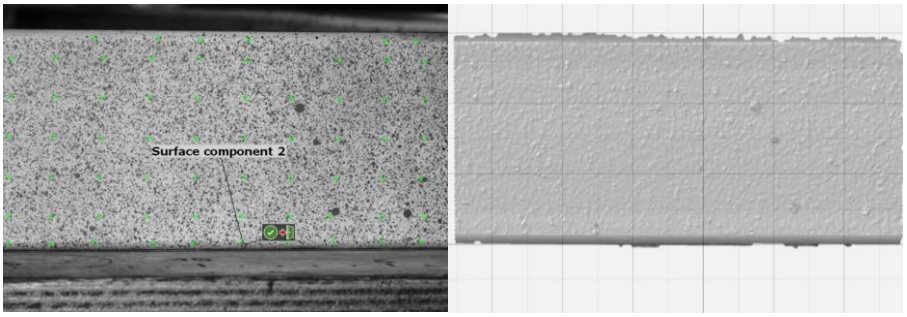

Figure 27. Surface created out of stochastic pattern by combining the facets

4.6 **FEM modeling**

A CAD model was designed in Creo parametric and transferred to ANSYS as STEP file. FEM was designed based on 3D model and bilinear isotropic plastic hardening. Basic mechanical property parameters of thin-walled rectangular steel alloy (C,H) E220 tube have been obtained, such as elastic modulus *E=210* G*Pa*, Poisson ratio v=0.3, density=7 g/mm3, coefficient of extension and yield and ultimate tensile strength, through uniaxial tensile test (SSAB hand book 2016). The material hardening behavior is expressed using the power exponent and tangent modulus calculated from the difference between ultimate and yield stress divided by strain assumed to be 100 MPa, close to perfectly plastic material. The dies are assumed to be rigid, while the rectangular tube is the deformable body. Table 7 depicts the material properties for the tubes.

Table 7. Material properties of SSAB E220 cold rolled t: 2mm (220C2) t:1.5 (220c1.5) and hot rolled t: 2mm (220H2)

	Rp0.2	Rm	A
220C2	344	374	44
220H2	312	359	49
220C1.5	336	378	45

Contact surfaces defined as frictional, meshing model and size were defined. According to the different sequence of tool movement in RDB process, the process parameters while bending were: bending angle (α) was 45 & 90°. Bending was based on implicit (time independent model) and was divided into different stages 3 for a 45 degree and 6 for a 90 degree bend accordingly. A displacement of Pressure die was chosen to be higher than the bend die to produce pressure on extrados of the tube and reduce thinning and potential deformation. Extra movement of the pressure die was compensated by frictional sliding on the tube. The bend die radius in the actual test was 50mm, in the FEM model to compare the effect of bend radius on the cross section three radius (50, 75 and 100 mm) were chosen.

Table 8. Mesh and contact parameters

	mesh method	element size (mm)	contact with tube
tube	tetrahedron	4	
bend die	quadratic	5	Frictional μ=0.5
wiper die	quadratic	5	Frictional μ=0.1
pressure die	quadratic	5	Frictional μ=0.2

Symmetric theory was used for FEM analysis and the model was cut into half as illustrated in Figure 28. (Logan 2000, 376).

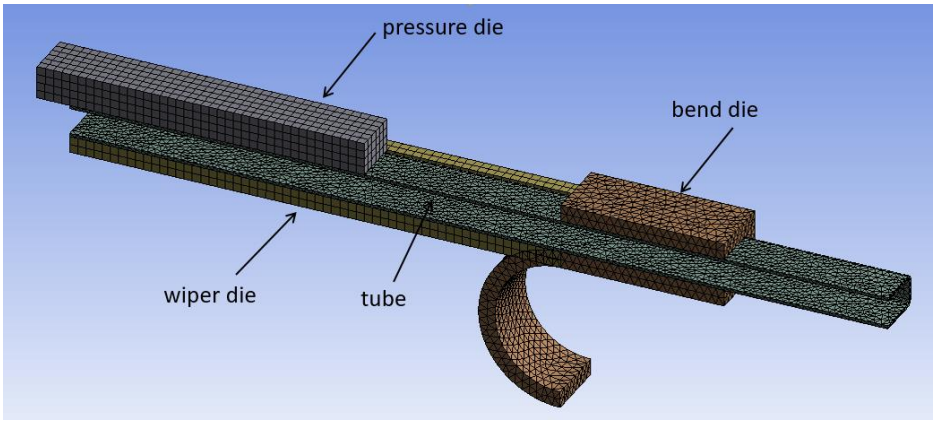

Figure 28. FEM model and mesh representation

5 RESULTS

5.1 ATOS draw bending results

5.1.1 Along the bending direction

Results shown in the Figures 29 and 30 are the concavity in the longitudinal line in the middle of the tube from 0 to 90 (every 10 degrees) and 0 to 45 (every 5 degrees) to the direction of the draw bending. For simplification acronyms used in the graphs represented tube and mandrel combinations. 220 cold rolled with old mandrel (C2_old), 220 hot rolled with old mandrel (H2_old), 220 cold rolled with new mandrel (C2_new), 220 hot rolled with new mandrel (H2_new) and 220C t=1.5 was bent using only one mandrel (C1.5).

Scanning result showed that the maximum concavity in a 90 degree bend occurred in cold rolled t=2mm tube while using the old mandrel and the minimum was seen in t=1.5 mm tube with 0.38 and -0.12 respectively. A Similar result was seen in 45 degree bend however hot rolled showed the same concavity but in a larger angle. Generally bends with new mandrel showed lower value of concavity.

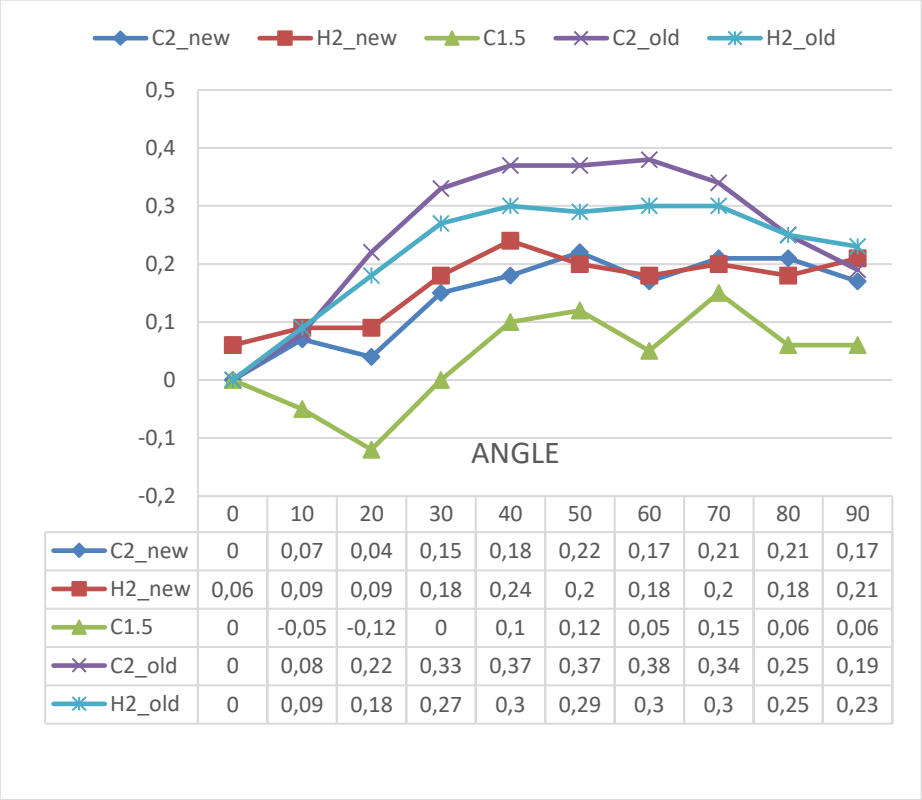

	0	10	20	30	40	50	60	70	80	90
C2_new	0	0,07	0,04	0,15	0,18	0,22	0,17	0,21	0,21	0,17
H2_new	0,06	0,09	0,09	0,18	0,24	0,2	0,18	0,2	0,18	0,21
C1.5	0	-0,05	-0,12	0	0,1	0,12	0,05	0,15	0,06	0,06
C2_old	0	0,08	0,22	0,33	0,37	0,37	0,38	0,34	0,25	0,19
H2_old	0	0,09	0,18	0,27	0,3	0,29	0,3	0,3	0,25	0,23

Figure 29. Concavity value in a 90 degree draw bending along the bend

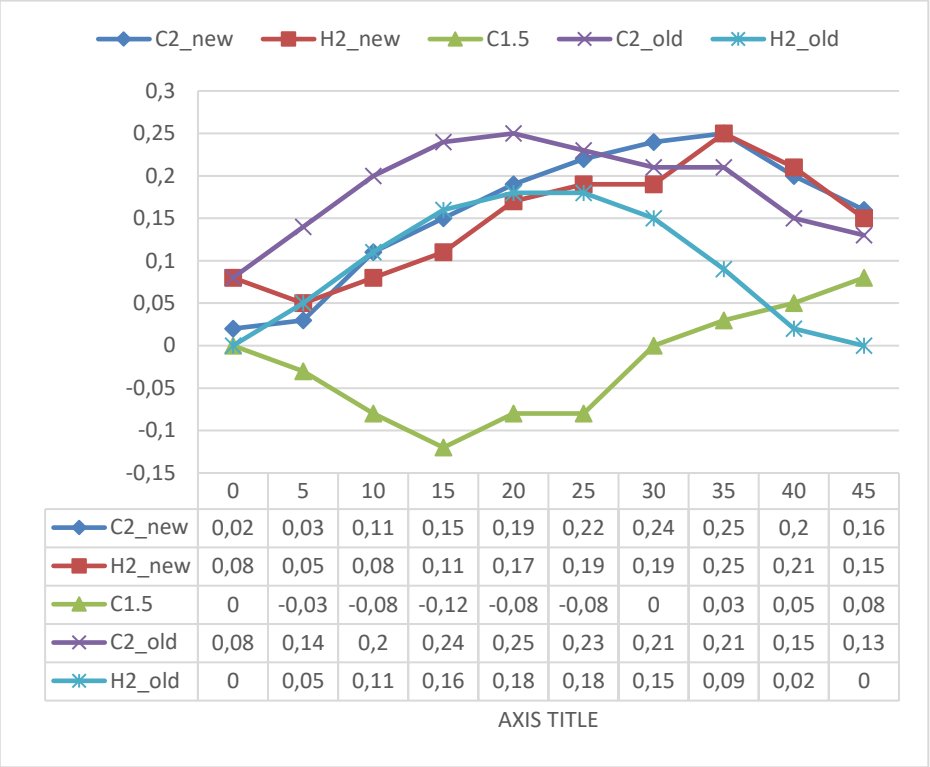

	0	5	10	15	20	25	30	35	40	45
C2_new	0,02	0,03	0,11	0,15	0,19	0,22	0,24	0,25	0,2	0,16
H2_new	0,08	0,05	0,08	0,11	0,17	0,19	0,19	0,25	0,21	0,15
C1.5	0	-0,03	-0,08	-0,12	-0,08	-0,08	0	0,03	0,05	0,08
C2_old	0,08	0,14	0,2	0,24	0,25	0,23	0,21	0,21	0,15	0,13
H2_old	0	0,05	0,11	0,16	0,18	0,18	0,15	0,09	0,02	0

Figure 30. Concavity value in a 45 degree draw bending along the bend

5.1.2 Along transverse direction

Results illustrated that the tube exactly follow the shape of the mandrel. Where mandrel is concave tube shows less concavity and where there is a groove (joints in mandrel) the concavity is higher. Results are shown in Figure (32 and 33). Tubes with 1.5 mm thickness where excluded from transverse measurement due to the very small amount of deformation as you see in Figure 31.

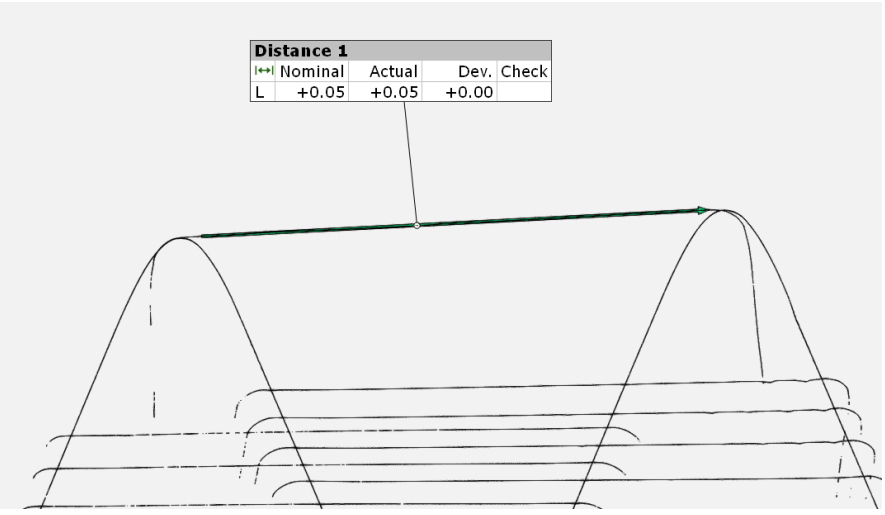

Figure 31. Concavity in the tube with 1.5 mm thickness (5 mm away from the center line)

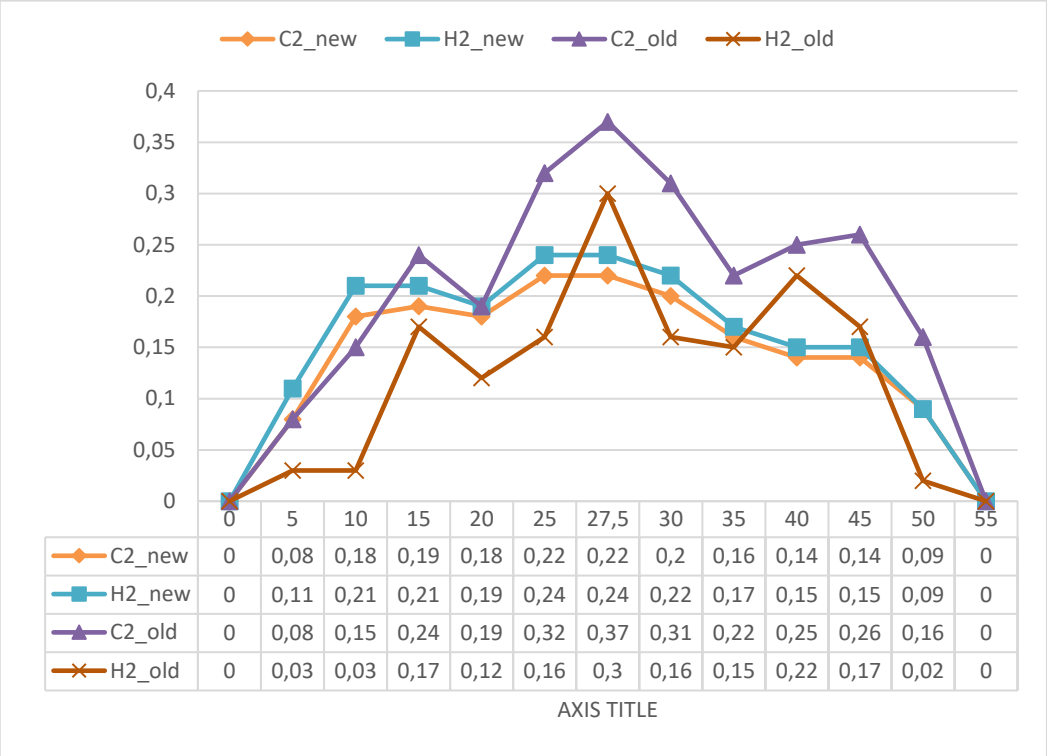

	0	5	10	15	20	25	27,5	30	35	40	45	50	55
C2_new	0	0,08	0,18	0,19	0,18	0,22	0,22	0,2	0,16	0,14	0,14	0,09	0
H2_new	0	0,11	0,21	0,21	0,19	0,24	0,24	0,22	0,17	0,15	0,15	0,09	0
C2_old	0	0,08	0,15	0,24	0,19	0,32	0,37	0,31	0,22	0,25	0,26	0,16	0
H2_old	0	0,03	0,03	0,17	0,12	0,16	0,3	0,16	0,15	0,22	0,17	0,02	0

Figure 32. Concavity value in a 90 degree draw bending in transverse direction. It can be seen that the cross section follows the shape of the mandrel by waving up and down.

	0	5	10	15	20	25	27,5	30	35	40	45	50	55
C2_new	0	0,09	0,18	0,18	0,16	0,2	0,24	0,23	0,16	0,21	0,23	0,1	0
H2_new	0	0,08	0,18	0,16	0,17	0,24	0,25	0,24	0,2	0,26	0,25	0,15	0
C2_old	0	0,05	0,08	0,18	0,11	0,13	0,28	0,14	0,14	0,23	0,19	0,065	0
H2_old	0	0,01	0,05	0,08	0,01	0,14	0,18	0,13	0,05	0,13	0,18	0,14	0

Figure 33. Concavity value in a 45 degree draw bending in transverse direction. It can be seen that the cross section follows the shape of the mandrel by waving up and down.

5.2 **ATOS Roll bending results**

There is no specific angle in roll bending in which the maximum concavity occur, instead a same amount of concavity happen along the bend direction. However here the same as the draw bending cold rolled tubes showed slightly a higher amount of concavity. Tubes with 1.5 mm thickness were failed during the bending process due to excessive wrinkling and were excluded from the process. In roll bending there was no mandrel in use during the bending and therefore the concavity in transverse direction show a perfectly curved shape with a maximum value in the middle (Figure 34-36).

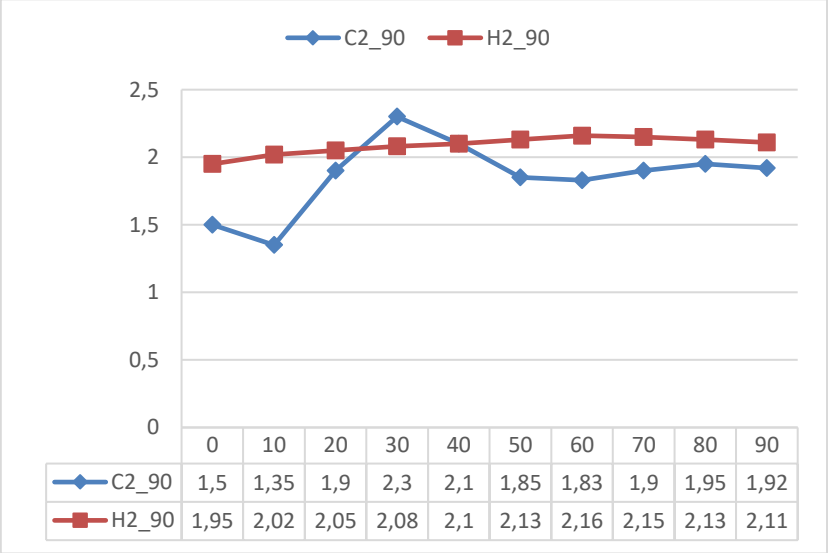

	0	10	20	30	40	50	60	70	80	90
C2_90	1,5	1,35	1,9	2,3	2,1	1,85	1,83	1,9	1,95	1,92
H2_90	1,95	2,02	2,05	2,08	2,1	2,13	2,16	2,15	2,13	2,11

Figure 34. Concavity value in a 90 degree roll bending along the bending direction

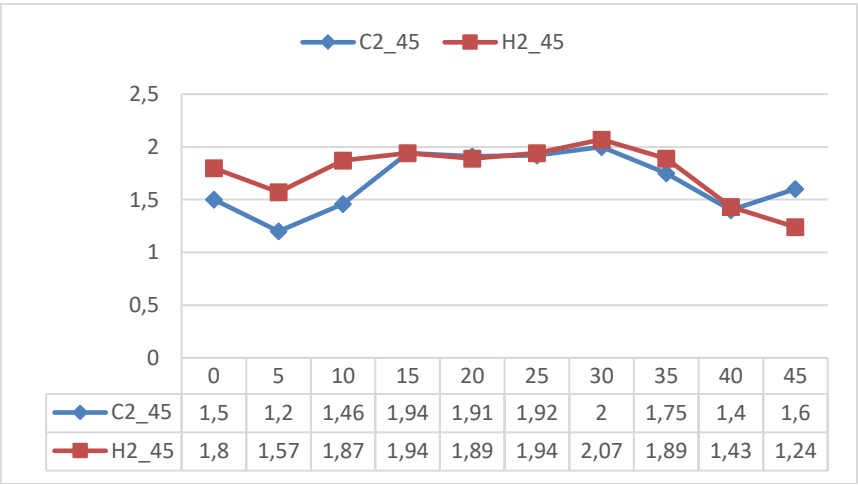

	0	5	10	15	20	25	30	35	40	45
C2_45	1,5	1,2	1,46	1,94	1,91	1,92	2	1,75	1,4	1,6
H2_45	1,8	1,57	1,87	1,94	1,89	1,94	2,07	1,89	1,43	1,24

Figure 35. Concavity value in a 45 degree roll bending along the bending direction

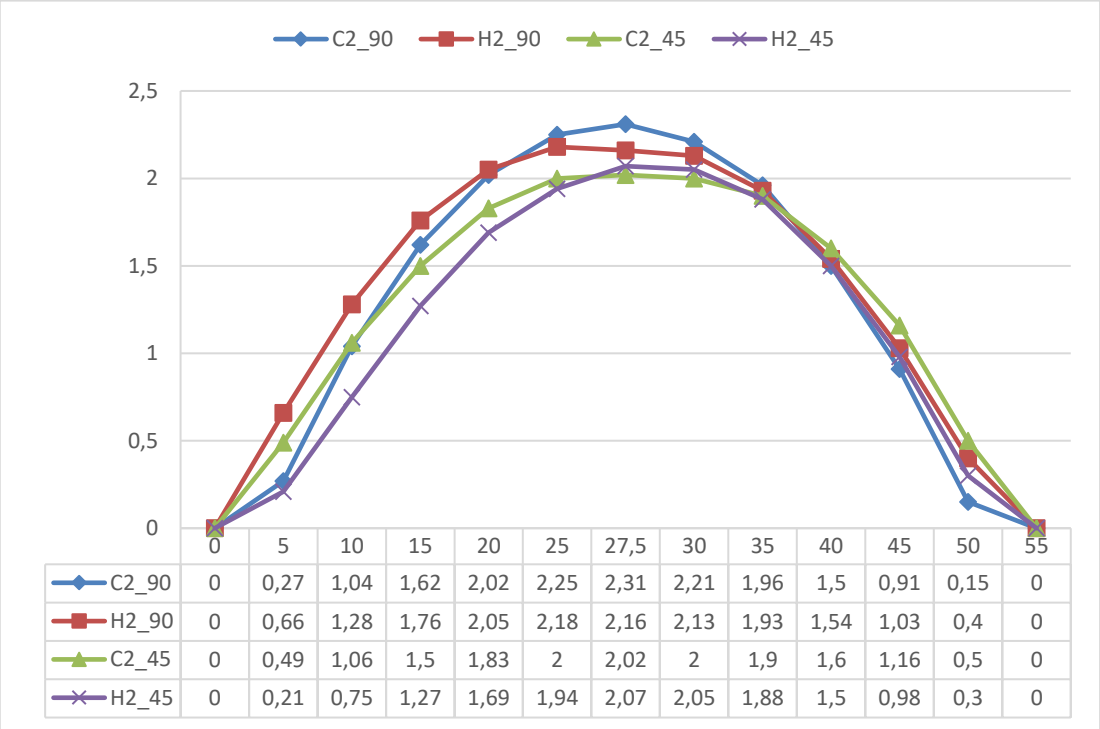

	0	5	10	15	20	25	27,5	30	35	40	45	50	55
C2_90	0	0,27	1,04	1,62	2,02	2,25	2,31	2,21	1,96	1,5	0,91	0,15	0
H2_90	0	0,66	1,28	1,76	2,05	2,18	2,16	2,13	1,93	1,54	1,03	0,4	0
C2_45	0	0,49	1,06	1,5	1,83	2	2,02	2	1,9	1,6	1,16	0,5	0
H2_45	0	0,21	0,75	1,27	1,69	1,94	2,07	2,05	1,88	1,5	0,98	0,3	0

Figure 36. Concavity value in roll bending in transverse direction

5.3 **ATOS bending without mandrel result**

Due to the limitation of number of elements I was not able to model the mandrel in ANSYS, hence bending process was simulated without mandrel. To be able to compare the results with FEM analysis I also bended the tubes without mandrel. We only could use 50 mm bend die radius during the bending process due to lack of any other bend die tool. The concavity was measured only in the middle of the bend angle and at the point in the middle of the transverse line. Figure 37 and 38 illustrate the position of the measuring value.

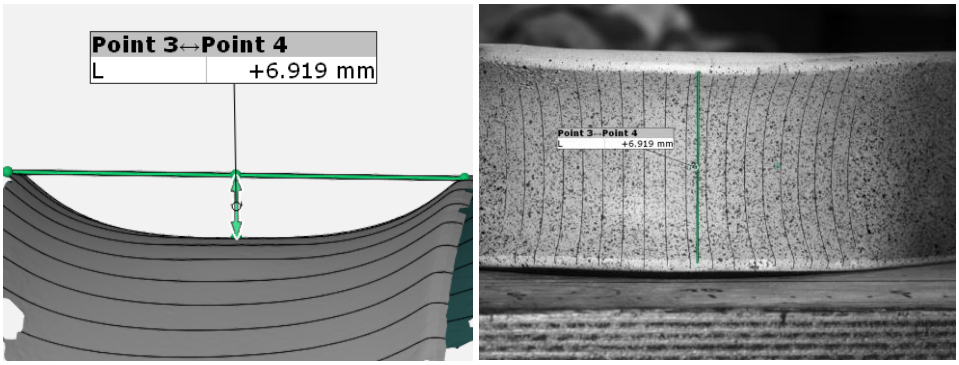

Figure 37. Concavity in the middle of the bend angle in a 90 degree draw bending

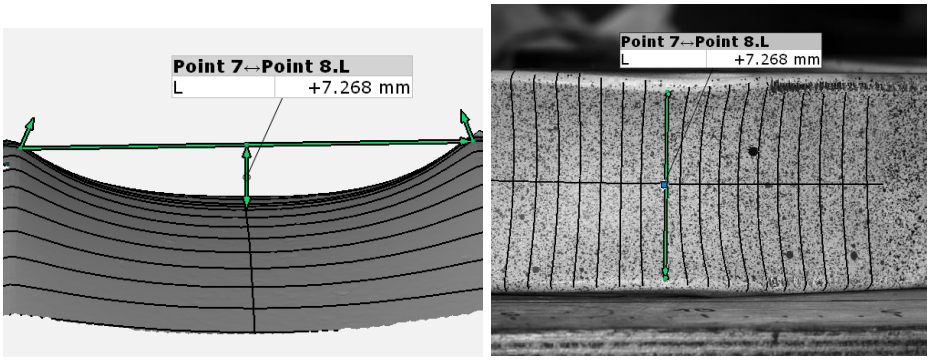

Figure 38. Concavity in the middle of the bend angle in a 45 degree draw bending

5.4 **ARAMIS results**

Strain in tube during the bending was measure with ARAMIS. To compare the result with FEM analysis only the result of bending without using mandrel is reported here. Von Mises strain was measured in three different location, first on surface of the tube, in the middle line along the bend direction (longitudinal) and in the line along the width of the tube in the middle of the bend angle (transverse). Result show that strain increases until it reaches the maximum in the middle of the bend angle and then decreases. Maximum strains were seen on the edges of the tube close to the middle of the bend angle. Figure 39-44 show the results.

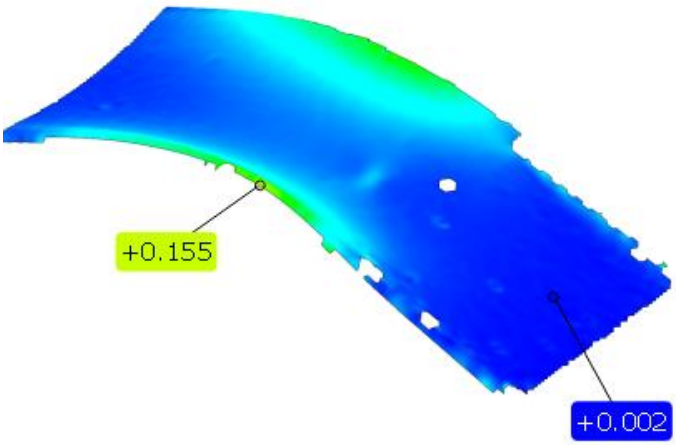

Figure 39. maximum and minimum strain in 45 degree draw bending

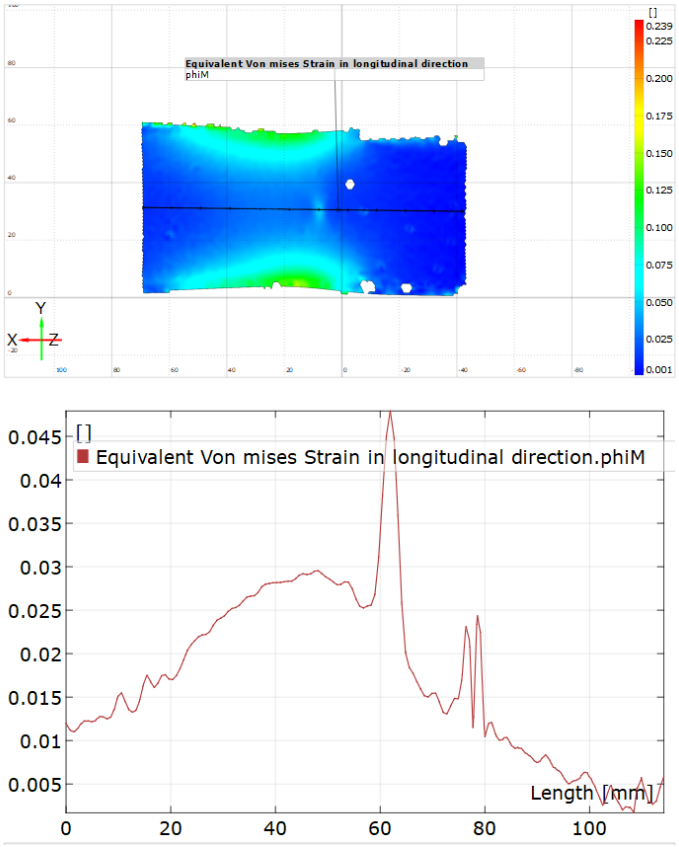

Figure 40. Longitudinal Von Mises strain in 45 degree draw bending

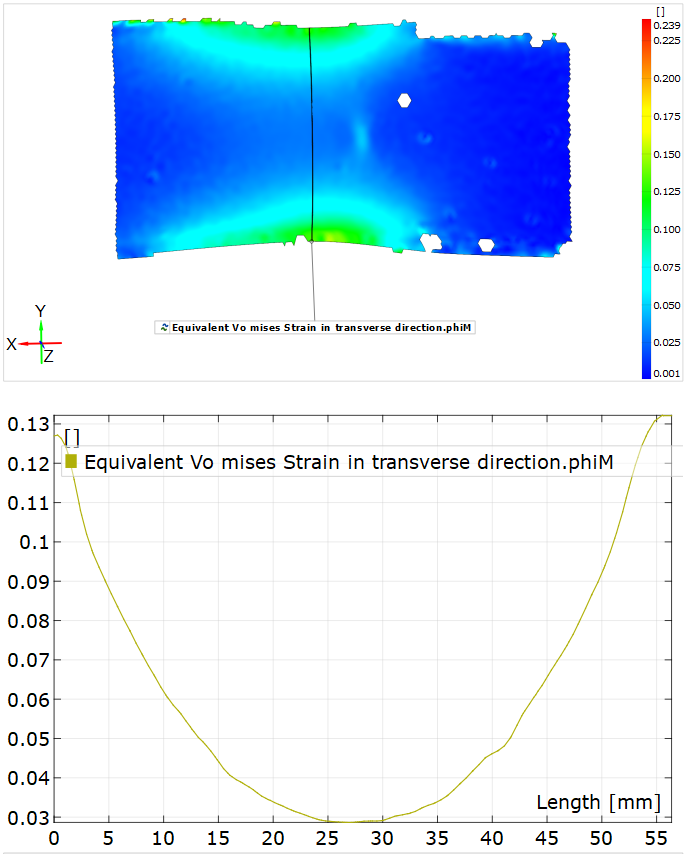

Figure 41. transversal Von Mises strain in 45 degree draw bending

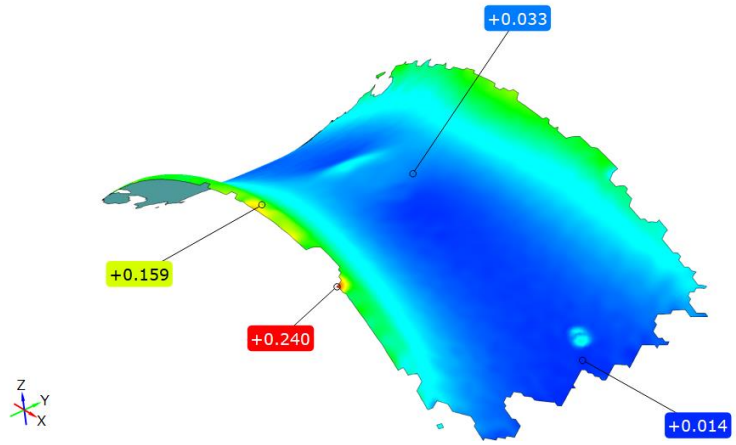

Figure 42. maximum and minimum strain in 90 degree draw bending

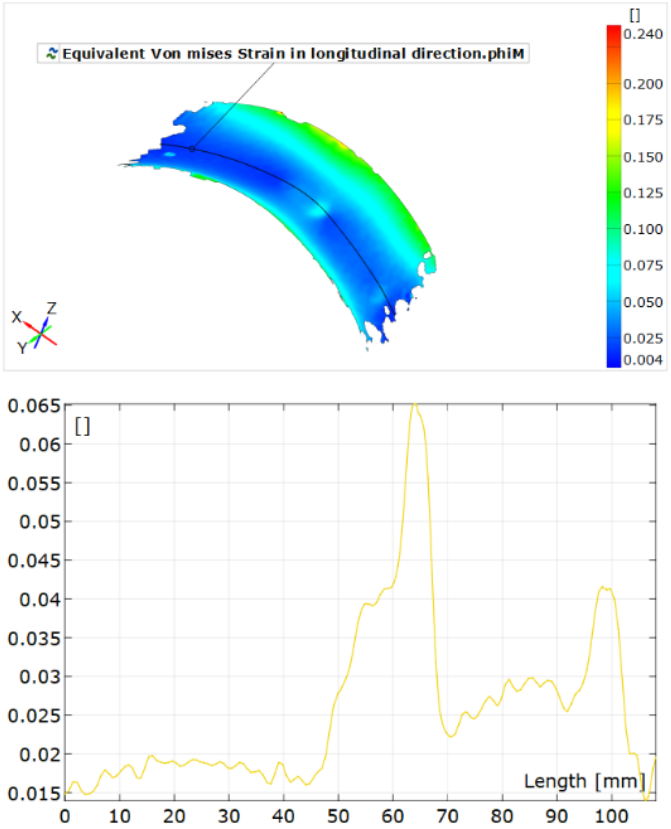

Figure 43. Longitudinal von Mises strain in 90 degree draw bending

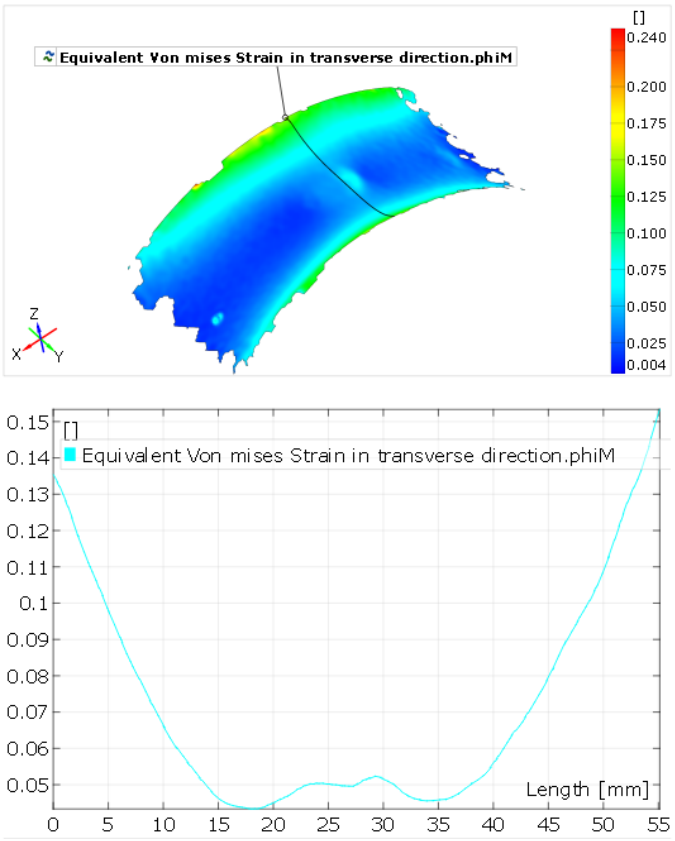

Figure 44. transversal von Mises strain in 90 degree draw bending

5.5 **FEM simulation results**

5.5.1 Similar bending radius

FEM analysis result includes, von Mises strain, concavity value in the middle of the bend angle and the general shape of the tube after bending. No direct way could be found to get the concavity value, therefore, the displacement in the middle of the tube were derived by two path component one in the side (edge) of the tube and one in the middle and displacement in X,Y direction after bending were measured. Displacement in z direction were neglected to assume two point are in the same plane. Figure 45-47 illustrate the result of FEM analysis. The distance between two points after deformation were calculated by this formula: $A = \sqrt{(x2 - x1)^2 + (y2 - y1)^2}$

Results of the concavity were:

45 degree bend: 6.18 mm

90 degree bend: 5.93 mm

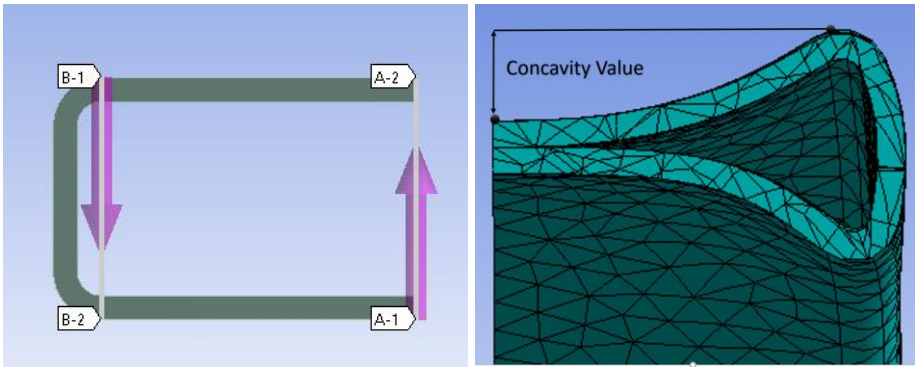

Figure 45. Cross section in the middle of the bend shows paths and measured distance before and after bending (45 degree bend)

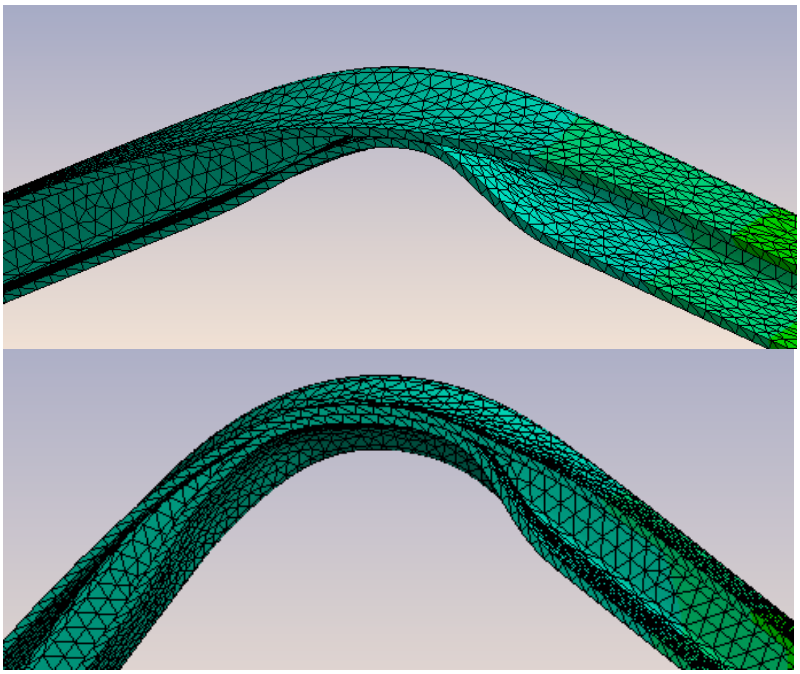

Figure 46. General view of the tube (up: 45 degree down: 90 degree)

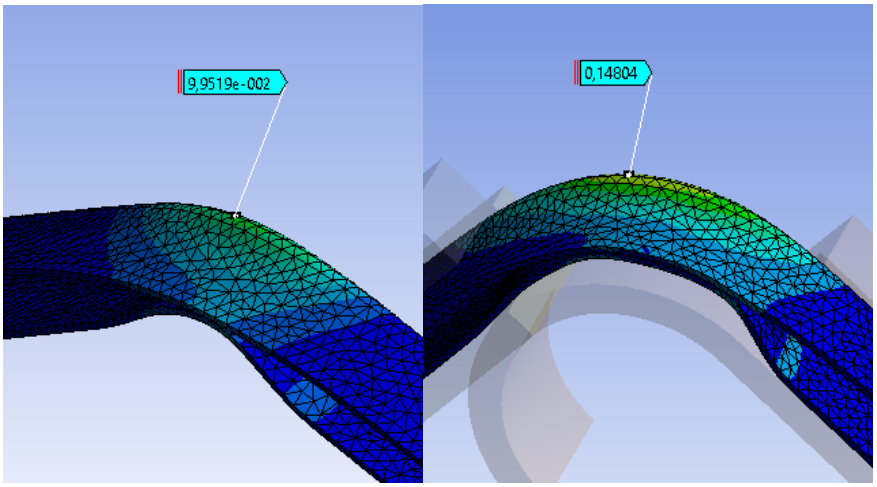

Figure 47. Maximum strain (με) (right: 90 degree and left: 45 degree bending)

5.5.2 Bigger bending radius

To see the effect of the bend radius on the cross section, two FEM models were designed with 75 and 100 mm bending radius. General view of the result are demonstrated in Figure (48 & 49).

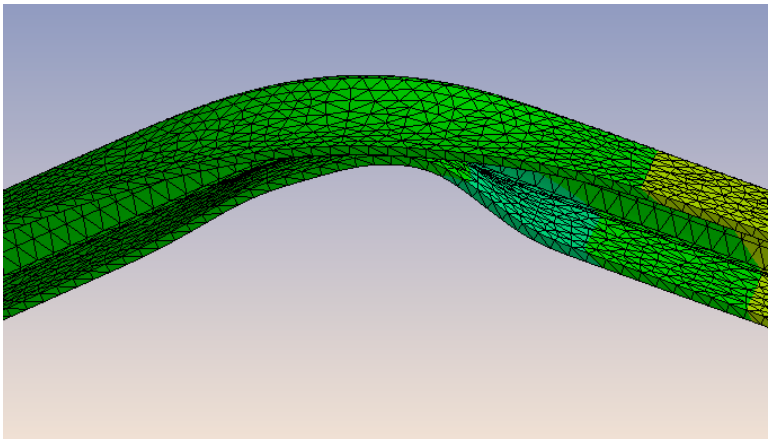

Figure 48. General view bending radius 75 mm, bend angle 45 degree

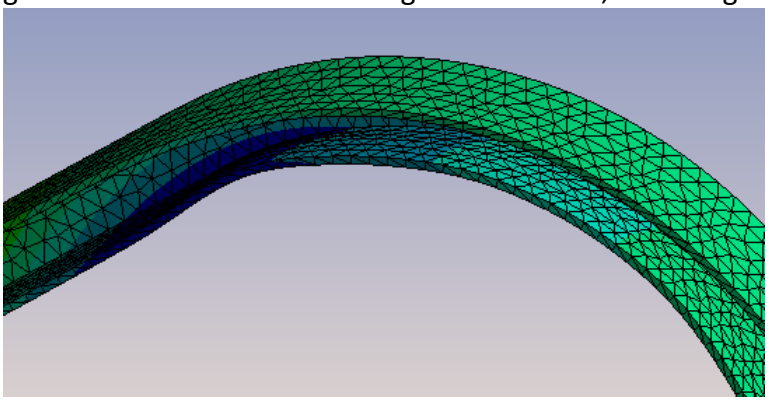

Figure 49. General view bending radius 100 mm, bend angle 90 degree

6 DISCUSSION

6.1 Effect of mandrel

Experimental result of draw bending with mandrel showed that cross sectional deformation in tubes besides the set up parameters such as clearance between pressure die and wiper die with tube, speed of the tube which were kept the same for all the bending, follow the shape of the mandrel. This effect can be seen in the difference of concavity using old mandrel vs new mandrel. This effect also acts in a similar way in the transverse direction were concavity increase and decrease following the shape of the mandrel. Looking at the old mandrel we can see that dimensions are reduced due to the frictional contact and wearing off over the time while new mandrels are yet fit. Figure 50 show the difference between bend result with mandrel and without mandrel.

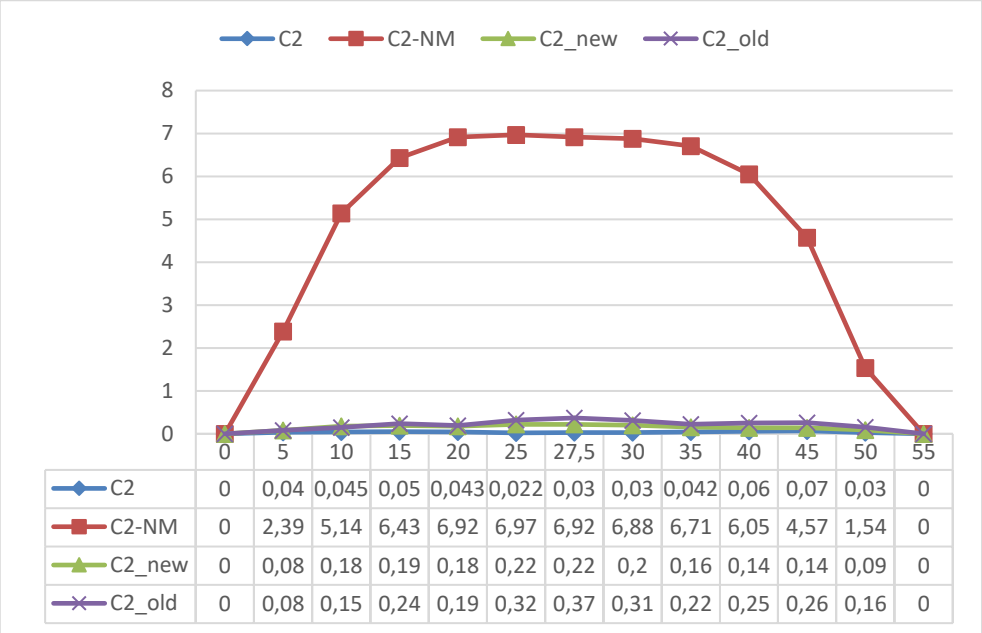

	0	5	10	15	20	25	27,5	30	35	40	45	50	55
C2	0	0,04	0,045	0,05	0,043	0,022	0,03	0,03	0,042	0,06	0,07	0,03	0
C2-NM	0	2,39	5,14	6,43	6,92	6,97	6,92	6,88	6,71	6,05	4,57	1,54	0
C2_new	0	0,08	0,18	0,19	0,18	0,22	0,22	0,2	0,16	0,14	0,14	0,09	0
C2_old	0	0,08	0,15	0,24	0,19	0,32	0,37	0,31	0,22	0,25	0,26	0,16	0

Figure 50. Cross sectional distortion comparison between tube before bending (C2), and after bending with new, old and without mandrel (C2-NM) in transverse direction in C2, 90 degree bend angle

Effect of mandrel is absolutely clear but how much new mandrel can improve the bend quality is directly depend on the quality of the mandrel and how precise are the dimensions compare to the tube's inner dimensions. One point here good to be consider and that is, even tube before bending has defects on the cross section. For that reason Figure 51 depict the cross sectional distortion after bending compare to the cross sectional distortions before bending using old and new mandrel. Maximum cross sectional distortion using the old mandrel is about 14 times more than tubes before bending compare to 8 times that of the new mandrel. Effect of tube grade on cross sectional distortion is neglectable.

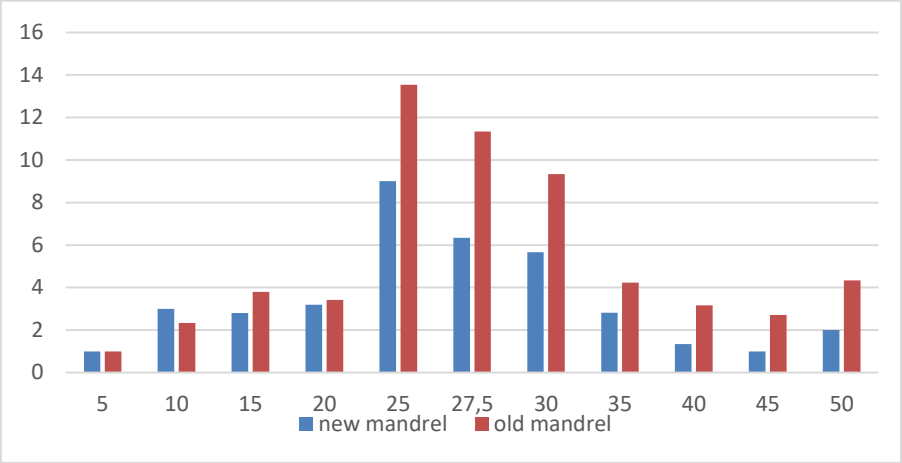

Figure 51. Cross sectional distortion after bending compare to the cross sectional distortions before bending using old and new mandrel.

6.2 Maximum cross sectional distortion

The maximum cross sectional collapse happened between 40 to 65 degree of the bend. This result confirming the result of the previous studies were, the maximum cross-sectional distortion reported to be at a position between 45°~ 60°. (Hongliang, Y 2016).

6.3 Minimum bend radius

Graph 52 shows the minimum bend radius for circular tubes. Experimental and FEM analysis show that bending square and rectangular tubes differs from bending circular tubes.

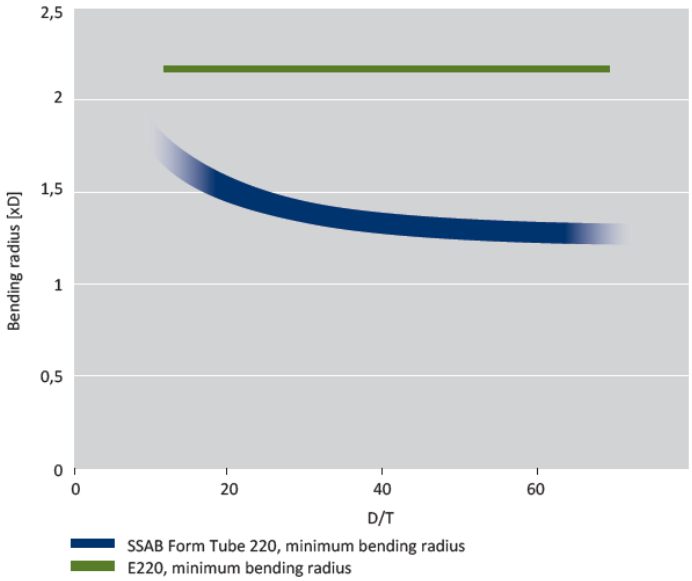

Figure 52. Minimum bending radius of SSAB Form Tube 220 vs. tube D/T ratio.

Roll bending result showed that for radiuses less than 400 mm (20xh) excessive wrinkling occur when height over thickness *(h/t)* is 10 and when t=1.5 wrinkling is unavoidable even with bigger radius (R=800 mm). FEM analysis showed that for R<5h the cross section completely collapse and make the bending impossible without mandrel. However for R>5h we can expect a concavity of around 3 mm (figure 53).
According to SSAB you can estimate bend radii using the equation:

$$CLR = 50 \times \frac{D}{A}$$

Where: *CLR* is centerline radius, *D* is tube diameter and *A* is elongation percentage. We get *R=1.2D* which does not comply with our case.

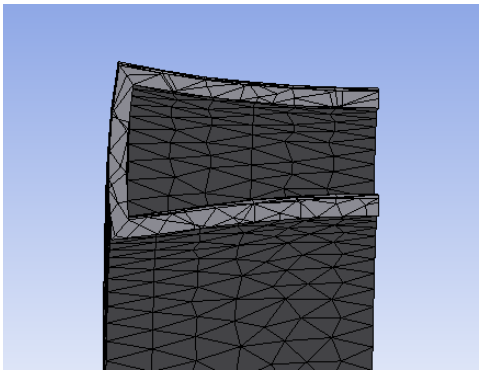

Figure 53. Cross section of the tube in the 45 degree of bend when bend radius is 100 mm

That is because rectangular tubes behave different than circular tubes. Work-hardened corners tend to increase minimum bending radius and the tube is more exposed to cross section changes: outer and inner surfaces have a tendency to concave, sides have a tendency to convex. Pocket bending is a common way to bend angular tubes, but they can also be bent without. Using draw bending, high quality tooling, ball mandrel and increased bending radius, it is possible to reach a bending radius down to 3 x tube height (3xD) with only a small cross sectional deformation (SSAB Precision steel tube 2016).

6.3.1 Effect of height and width

Moreover the ratio between height and width is an important factor in rectangular tube bending, B/H=60/20 in our study gives the possibility of minimum R>5h for minimum bending radius. While, Hongliang, Y etal 2016 reported the relative distortion of sections at every position with aspect ratio B/H= 40/30, the wall thickness t= 2mm, bending radius R= 90, 105, 120mm. Figure 54 shows the result of the cross sectional distortion in different bend radiuses. As we can see, the maximum value of the relative distortion appears mostly between 45~ 60° similarly, the relative values of the distortion in the width and height direction increases with the bending radius decreasing. However they were using the minimum radius of 3R and reported the distortion of around 1mm. Tian Shan in 2013 reported that

wrinkling is more prone to occur with the increase of b/h; while h kept unchanged, the cross-section distortion become bigger with the increase of b.

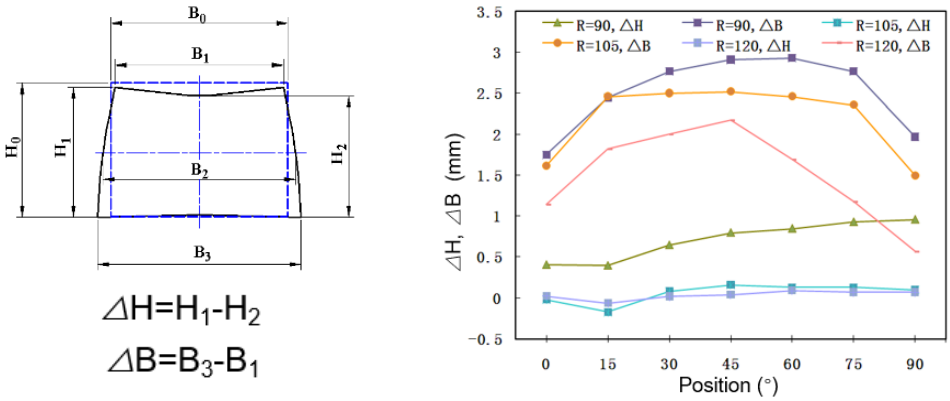

Figure 54. Influence of bending radius on cross sectional distortion, smaller bend radius cause bigger cross sectional distortion (Hongliang, Y etal 2016)

6.4 **The comparison between FEM and experimental results**

Concavity value in the experimental result are bigger than of the FEM results. 6.9 vs 5.9 in 90 degree bend angle and 7.2 vs 6.2 in 45 degree bend angle (Figure 55 & 56). The higher value in the 45 degree compare with the 90 degree bend angle is because of the wrinkling on the other side of the tube. In the 90 degree bend angle the other side of the tube deforms and collapse until it push the top surface and causes reduction in concavity which is similar in bot experimental and FEM result.

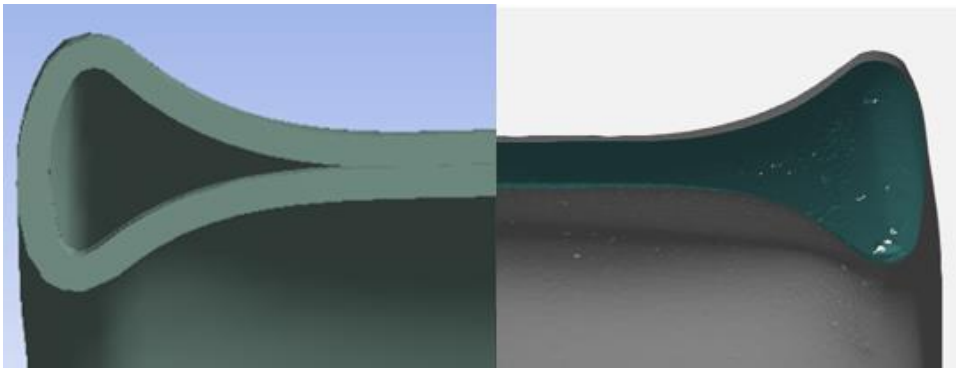

Figure 55. Cross sectional comparison of 90 degree bend in the 45 degree of the bend, FEM result (left) vs actual result (right).

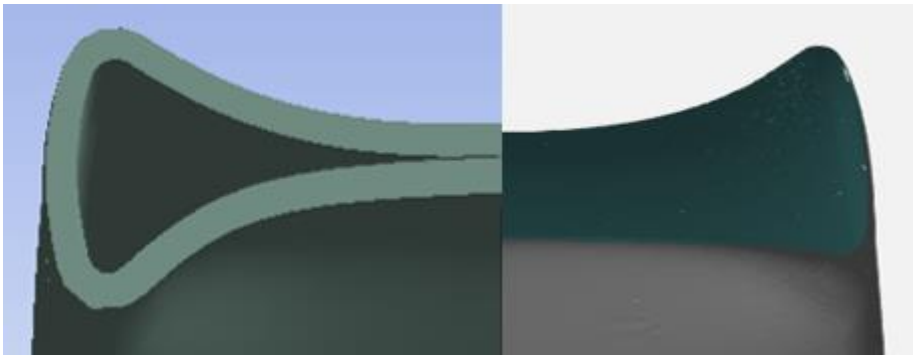

Figure 56. Cross sectional comparison of 90 degree bend in the 45 degree of the bend, FEM result (left) vs actual result (right).

The strain values from ARAMIS and FEM differs by small margin as can be seen in the Figure 57 and 58 by (0.15 vs 0.1 με) in the 45 degree bend and (0.24 vs 0.15 με) in the 90 degree bend angle.

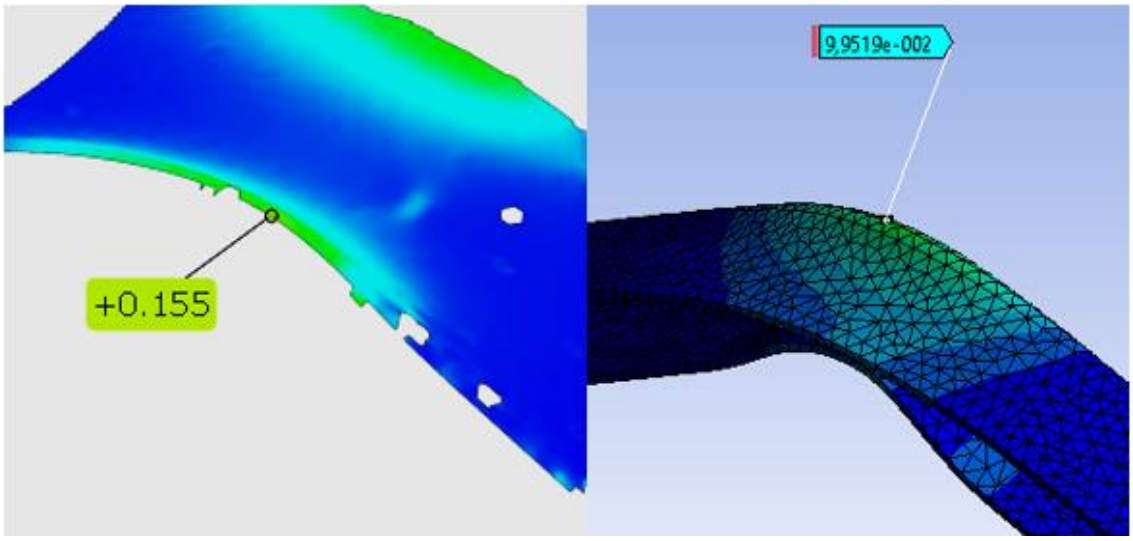

Figure 57. Maximum Von Mises strain comparison in 45 degree bend angle, actual sample (left) vs FEM result (right)

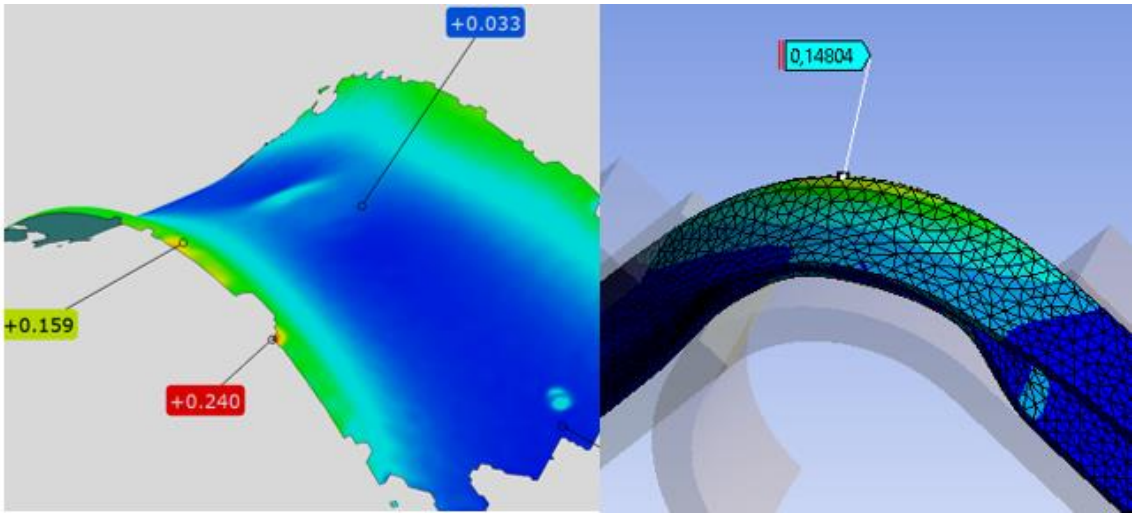

Figure 58. Maximum Von Mises strain comparison in 45 degree bend angle, actual sample (left) vs FEM result (right)

Shape of the cross section after bending, from longitudinal view differ from actual samples as it is depicted in the Figure 59 & 60. In FEM model collapse of the bottom side is smooth and no wrinkling is seen while the experimental samples show a wrinkle.

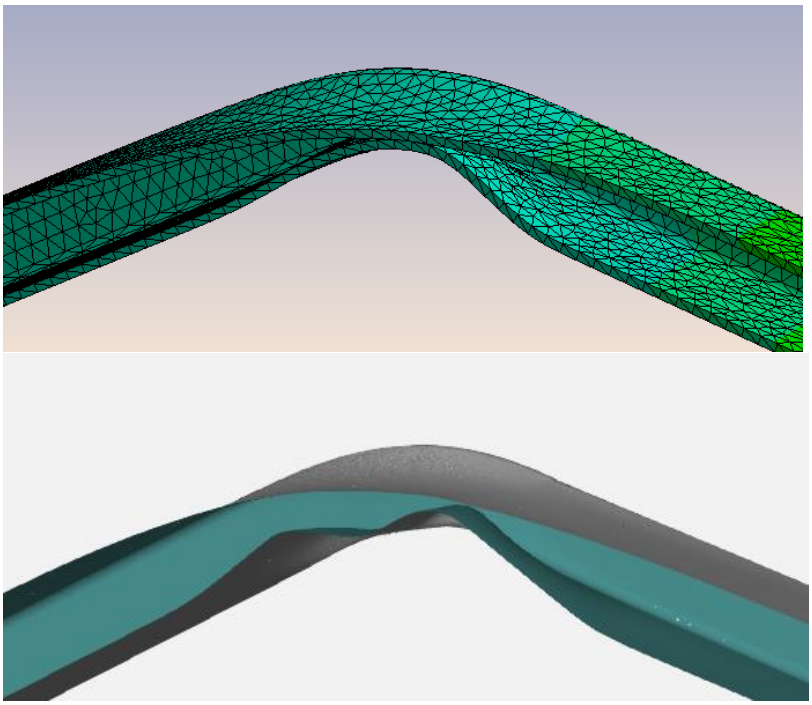

Figure 59. Shape comparison 45 degree bend angle FEM (top) vs actual sample mesh (down)

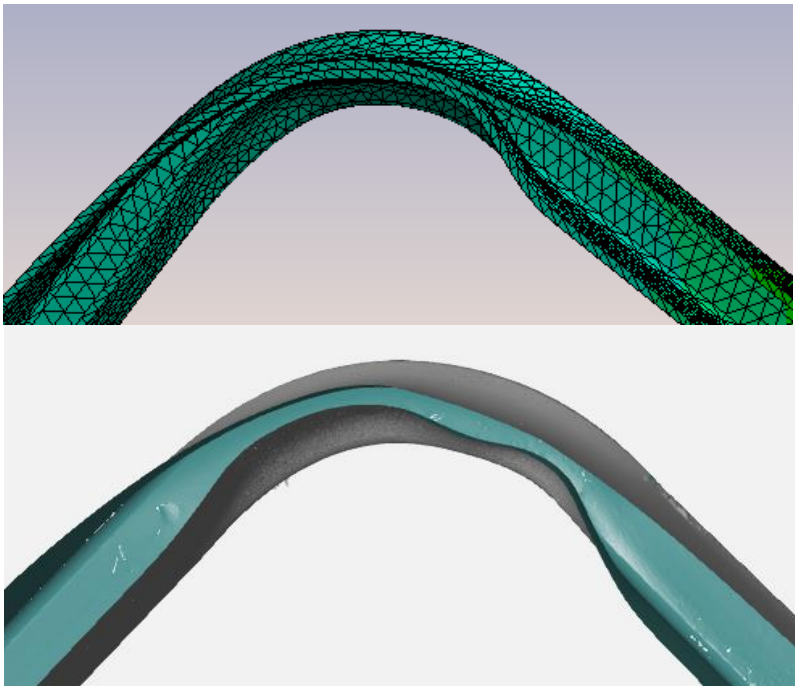

Figure 60. Shape comparison 90 degree bend angle FEM (top) vs actual sample mesh (down)

7 CONCLUSION

In rotary draw bending a good bending result is not possible without a mandrel, when it comes to rectangular tubes with B/H=60/20 and t=2 mm for a bend radius lower than 100 mm

Bending of rectangular tube with t=1.5 is not feasible using roll bending method.

In bending with a mandrel the quality of the mandrel and the clearances pretty much define the cross sectional deformation of the tube.

The reason behind the difference between the FEM result and the actual result can be due to the following factors:

Accurate material properties (stress strain behaviour of the tube) in FEM a simplified bilinear isotropic model was assumed.

Bending set up parameters and strain hardening due to the rate.

The pressure die displacement, which was greater in FEM than actual conditions and it can be assumed that the pushing force generated by the die reduces the thinning and tension on the extrados and result in lower strain and distortion values.

Aramis can be utilized for estimating the strain of the tube in multilinear conditions, thinning and Von Mises stress.

This thesis focused more on bending tubes using a mandrel in the RDB method. The FEM results showed that bending is achievable without cross sectional collapse when the bend radius is 100 mm. Unfortunately a limitation of this project was that, there was not a bend die with radius more than 50 mm for bending the tubes and to compare the results with the FEM results.

Finding the appropriate parameter for b, h and t and a minimum possible bend radius in roll bending and rotary draw bending can be useful for next projects.

REFERENCES

Ansys online tutorials, Retrieved 15 October 2018 from:
http://inside.mines.edu/~apetrell/ENME442/Labs/1301_ENME442_lab7.pdf

ARAMIS adjustable 5 manual, retrieved 24 January 2019:
http://webcache.googleusercontent.com/search?q=cache:1pxehqVI6L4J:materials-science.phys.rug.nl/index.php/home/downloads/category/1-manuals%3Fdownload%3D27%253Aaramis-v61.J+&cd=4&hl=en&ct=clnk&gl=fi

ATOS Compact manual: , retrieved 30 January 2019:
http://www.henindo.co.id/home/ATOS-Compact-Scan_EN_RevA.pdf

Bending retrieved 12 November 2018 from:
https://en.wikipedia.org/wiki/Bending

Corona, E. (2004). A simple analysis for bend-stretch forming of aluminum extrusions. International Journal Mechanical Sciences, 46(3), 433-448.

Li H, Yang H, Zhang Z.Y, Li G.J, Liu N, Welo T. (2014) Multiple instability-constrained tube bending limits. State Journal of Materials Processing Technology 214 (2014) 445– 455. https://doi.org/10.1016/j.jmatprotec.2013.09.027

Holm, H. (2002). The Finite Element Method - Theory. Retrieved 20 December 2018 from: http://illustrations.marin.ntnu.no/structures/analysis/FEM/theory/index.html

Hongliang, Y, Zhongwen, X and Hao, Z. (2016) The Impact of Geometric Parameter on the Cross Section Precision in Rotary Draw Bending of High-strength steel tube with rectangular section. Harbin Institute of Technology, Harbin, 8nd International Conference on Physical and Numerical Simulation of Materials Processing, ICPNS'16 Seattle Marriott Waterfront, Seattle, Washington, USA, October 14-17, 2016

Kervick, R.J., and Springborn, R.K., 1966, Cold Bending and Forming Tube and Other Sections, , Dearborn, MI. American Society of Tool and Manufacturing Engineers.

Liu, Y. L. (2007). 3-D FEM analysis of section distortion in bending process of the thin-walled rectangular tube. Journal of Plasticity Engineering, 14, 72-75.

Logan, D. (2000). A First Course In The Finite Element Method Third Edition, BROOKS/COLE.

Mendricky, R. (2016) Determination of Measurement Accuracy of Optical 3d Scanners. Technical University of Liberec Department of Manufacturing Systems and Automation. DOI: 10.17973/MMSJ.2016_12_2016183

Nikishkov G. P.(2004) Introduction To The Finite Element Method. Lecture Notes. University of Aizu, Aizu-Wakamatsu 965-8580, Japan.

Podaný K, Samek R, K. Matousek. Mechanics of Square Tubes Bending and Cross Section Distortion. MM science journal 2010. Retrived 8 November 2018 from: http://www.mmscience.eu/journal/issues/december-2010/articles

Paulsen, F., & Welo T. (2001). Cross-sectional deformations of rectangular sections in bending: Part II - analytical models. International Journal Mechanical Sciences, 43(1), 131-152.

Peng, H. L., & Li, M. Z., & Fu, W. Z., & Lan, Y. W. (2012). Numerical analysis of cross-section distortion of multi-point press bending for rectangular tube. Forging & Stamping Technology, 37(1), 87-90.

SSAB (2016). Precision Steel Tube Handbook (compilation of training material for bending welding and coating), retrieved 20 October 2018 from: https://www.ssab.ru/-/media/files/en/hollow-sections/cross-sectional-properties/precision-tubes-dimensions-and-cross-sectional-properties_4.pdf?m=20160219063340

Stres-Strain Retrieved 15 October 2018 from: https://en.wikipedia.org/wiki/Stress%E2%80%93strain_curve#cite_note-1

The fabricator (2014). Tube and pipe basics: How to achieve the perfect bend. Retrieved 12 October 2018 from: https://www.thefabricator.com/article/tubepipefabrication/tube-and-pipe-basics-how-to-achieve-the-perfect-bend

Tian, Liu, Yang. (2013) Effects of geometrical parameters on wrinkling of thin-walled rectangular aluminum alloy wave-guide tubes in rotary-draw bending, Chinese Journal of Aeronautics, 2013,26(1): 242–248

Utsumi, N., & Sakaki, S. (2002). Countermeasures against undesirable phenomena in the draw-bending process for extruded square tubes. Journal of Materials Processing Technology, 123(2), 264-269.

Yan J, Yang H, Zhan M, et al. Forming limits under multi-index constraints in NC bending of aluminum alloy thin-walled tubes with large diameters. Sci China Tech Sci, 2010, 53: 326-342, retrieved 2019 from: https://www.researchgate.net/publication/226453588_Forming_limits_under_multi-index_constraints_in_NC_bending_of_aluminum_alloy_thin-walled_tubes_with_large_diameters